spectroscopy (NIRS) chemometric calculation [6–13]. However, a unique analytical procedure using characteristic peaks based on crystal growth has not been reported, to the our knowledge.

Caira et al. [17] analyzed the chemical structure of two types of forms of TBR using X-ray diffraction. They described a crystal packing arrangement of two types of forms: Form 1 had a monoclinic prism containing four trimers of TBR in a unit cell, and Form 2 had a triclinic block containing two trimers in a unit cell. They concluded that the van der Waals attraction interactions (C—H···π) link trimers, and an intermolecular hydrogen bond (—OH···N) links three TBR molecules, composing a trimer.

These conclusions concerning the crystallographic structure of polymorphs based on the stereochemical observations suggest that a trimer is composed of two molecules that have the same absolute configuration (S-, R-, R-) at the chiral center and a molecule that has the opposite absolute configuration (R-, S-, S-).

The authors previously conducted quality analyses of TBR TDDS tape using microscopic laser Raman spectroscopic mapping (MLRSM) and terahertz pulsed imaging (TPI) [14,15]. In those studies, Raman chemical maps of crystalline TBR in matrices were obtained based on a characteristic peak, and the authors observed lumps of crystals in the terahertz images based on the change in a refractive index of terahertz pulse in the tape. In the present study, the authors observed the characteristic peak from 6500 cm^{-1} to 6350 cm^{-1} based on the crystal growth of TBR using NIRS. A simple data treatment which is not multivariate data processing but an integrated value (a peak area) of the absorption from 6500 cm^{-1} to 6350 cm^{-1} was applied. This absorption consists of overlapped three absorptions, but the origin of these absorptions is only an overtone of secondary amine. Moreover, required accuracy for estimation of crystallization ratio of TBR allows applying a simple data processing. The authors also examined the applicability of a non-destructive analysis for the quality control of TDDS tapes using NIRS and the feasibility of a time-course analysis of the distribution of TBR crystals in matrices by near infrared spectroscopic imaging (NIRI).

2. Experimental

2.1. Instruments and measurement conditions

NIRS measurements were performed using MPA Fourier-transform NIR spectrometer (Bruker Optik, Ettlingen, Germany). Microscopic NIRI measurements were performed using Vertex70 Fourier-transform infrared (IR) spectrometer (Bruker Optik) equipped with Hyperion 2000 IR Microscope (Bruker Optik). The resolution, scan numbers and measurement range were set at 2 cm^{-1}, 64, and 8000–4000 cm^{-1} for NIR, and 16 cm^{-1}, 32, and 8000–4000 cm^{-1} for NIRI, respectively. For NIR macroscopic mapping, MPA Fourier-transform NIR spectrometer was used, and NIR light was focused on the stage. The tapes were moved by 3 mm for each measurement. A total of 81 spectra were used to compose the macroscopic map. To reduce the total measurement time, the resolution and scan numbers were set at 16 cm^{-1} and 8, respectively. The measurement areas were 3 mm × 3 mm for the NIRI and 27 mm × 27 mm for the NIR macroscopic mapping. For the NIRI measurements, the liner was removed from the matrix. For the transmittance-reflectance measurements, a metallic board was put on the sample tapes.

2.2. Materials

Tulobuterol (TBR, purity > 99.0%, Fig. 1) was provided by Hisamitsu Pharmaceutical Co. (Tokyo, Japan). 2-Ethylhexyl acrylate vinylpyrrolidone copolymer, isopropyl myristate, polyisobutylene, polybutene, and lipocyclic petroleum resin for matrices of the model tapes were used as Japanese Pharmaceutical Excipients (JPE)-quality products. Hokunalin® Tape (1 mg and 2 mg) (Maruho Co., Osaka, Japan) and other TBR tape products were purchased from a commercial source. Carbon tetrachloride as a reagent grade was purchased from commercial source.

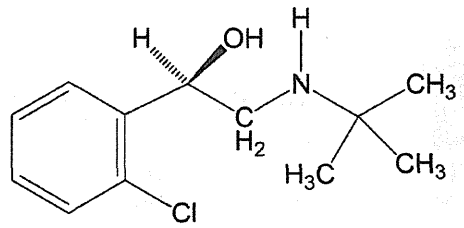

Fig. 1. Chemical structure of tulobuterol (TBR).

2.3. Preparation of model tapes

The model tapes were prepared by the TDDS Laboratory (Hisamitsu Pharmaceutical Co.). To identify lumps of TBR crystals in the matrix, the authors prepared two types of matrix for model tape: a rubber matrix and an acrylic matrix. These two kinds of matrix are commonly used for a transdermal tape. In order to analyze a commercial tape which is made from an acrylic or a rubber matrix, model tapes made from these matrices should be prepared. TBR and other ingredients were added in a mortar and thoroughly stirred. The mixture was spread on a liner, and residual solvents were removed by drying. The matrix was adjusted to a constant thickness (approximately 50 μm) and pasted onto a supporting board. A polyethylene terephthalate (PET) film was selected for both the liner and the supporting board of the model tapes. Each sample was cut to a size of 36-mm dia. TBR crystals in the model tapes were generated by leaving the samples to stand for one week (for the rubber matrix) or one month (for the acrylic matrix).

Model tapes containing 0% (w/w) (R-0, placebo) or 10% (w/w) (R-10) of TBR in the rubber matrix (consisting of polyisobutylene, polybutene, and lipocyclic petroleum resin) were prepared. The authors observed small white crystals in all areas of the matrix of the R-10 sample. Model tapes containing 0% (w/w) (A-0, placebo), 20% (w/w) (A-20) or 30% (w/w) (A-30) of TBR in the acrylic matrix (composed of an acrylic adhesive polymer and isopropyl myristate) were prepared. Due to the solubility of TBR, higher TBR concentrations were necessary to generate crystals in the acrylic matrix than in the rubber matrix.

2.4. Data treatment

The spectral data was treated using the software OPUS 6.5 (Bruker Optik). Standard normal variate (SNV) normalization and second derivative of spectra were carried out as a data pre-processing. NIR chemical images and maps are constructed using integrated values of absorption from 6500 cm^{-1} to 6350 cm^{-1}. Integrated values were calculated using the attached software OPUS 6.5.

2.5. Preparation of TBR carbon tetrachloride solution and NIR measurement

The authors prepared 0.5% (w/v) and 10% (w/v) TBR carbon tetrachloride solutions. A suitable volume of each solution was put in a cuvette and measured by a transmittance NIR spectrometer using carbon tetrachloride as a reference. The measurement range,

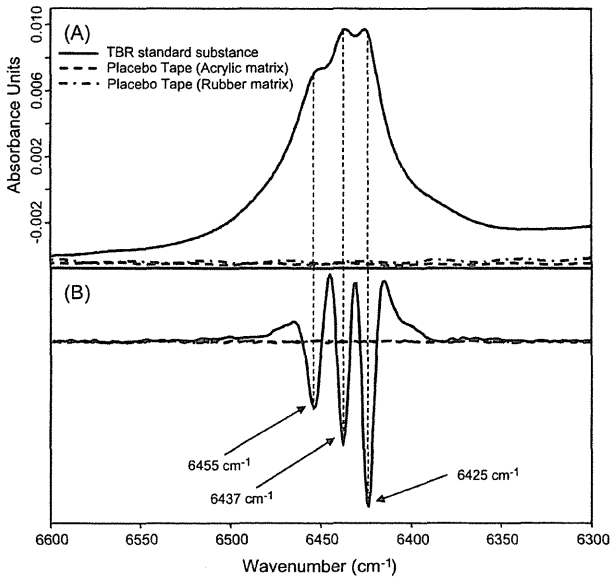

Fig. 2. NIR spectra of TBR reference standard and placebo tapes (TBR 0%). (A) Baseline correlated NIR spectrum and (B) second derivative NIR spectrum.

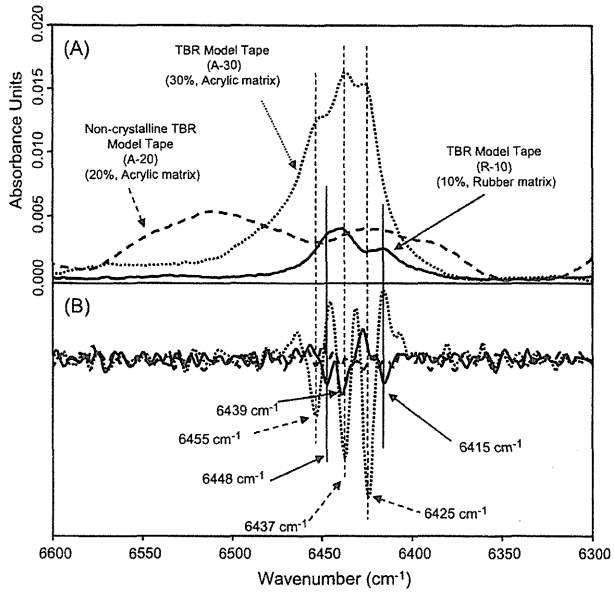

Fig. 3. NIR spectra obtained from the A-30, A-20, and R-10 model tapes. (A) Baseline correlated spectra and (B) second derivative spectra.

resolution, and scan number were set at 8000–4000 cm^{-1}, 2 cm^{-1}, and 64, respectively.

2.6. Preparation of amorphous form of TBR

To make an amorphous TBR, a portion of crystalline TBR (m.p.: 90.4 °C) on a glass dish was put into a dryer (the temperature was set at 100 °C). After crystalline TBR was melted, heating was stopped. And the glass dish was left for a while under an ambient temperature. A melting point of melted TBR was checked by a differential scanning calorimetry (DSC) (82.6 °C).

3. Results and discussion

3.1. Characteristic absorption based on the crystallization of TBR

Fig. 2 shows the base-line correlated NIR spectrum and the second derivative NIR spectrum of pure TBR and the placebo model tapes (rubber matrix R-0 and acrylic matrix A-0). The characteristic peak of TBR was observed from 6500 cm^{-1} to 6350 cm^{-1}, and there was no interfering peak around it. The second derivative absorption of the peak was divided into three sharp peaks at 6454 cm^{-1}, 6437 cm^{-1} and 6423 cm^{-1}. The second derivative peak which had the strongest intensity, was observed at 6423 cm^{-1}.

The offset spectra and the second derivative spectra obtained from the A-30, A-20, and R-10 model tapes are shown in Fig. 3. The TBR characteristic peak from 6500 cm^{-1} to 6370 cm^{-1} was detected in the A-30 model tape, which had white crystals in the matrix. The three sharp peaks at 6455 cm^{-1}, 6437 cm^{-1} and 6425 cm^{-1} were also observed on the second derivative spectrum. These peaks correspond to pure TBR. Although the absorption from 6500 cm^{-1} to 6350 cm^{-1} was also observed on the spectrum obtained from the R-10 model tape (which contained white crystals), the peak shape of R-10 was a bit different from that of A-30. There are three peaks on the second derivative spectrum of first overtones of N–H, and their peak positions were observed at 6448 cm^{-1}, 6439 cm^{-1} and 6415 cm^{-1}. The peak positions (apart from the center peak) were shifted to 7 cm^{-1} or 10 cm^{-1} lower peak positions.

The unique absorption was not detected on the spectrum obtained from the A-20 model tape (which did not contain white crystals in the matrix). TBR molecules in the A-20 matrix may remain in an amorphous form and/or at a very early stage of their crystallization process. The authors suspect that the broad waveform observed on the spectrum obtained from A-20 (Fig. 3) is a fringe. These results suggest that the peak from 6500 cm^{-1} to 6350 cm^{-1} is uniquely produced by the crystallization of TBR. The NIR absorptions of TBR that are assigned from a group vibration and a chemical structure are shown in Table 1.

3.2. Vibrational spectroscopic understanding of the characteristic absorption of TBR crystals

Fig. 4 shows the vector normalized and second derivative spectra obtained from the TBR carbon tetrachloride (CCl_4) solutions at 0.5% (w/v) and 10.0% (w/v). In the spectrum obtained from the 0.5%

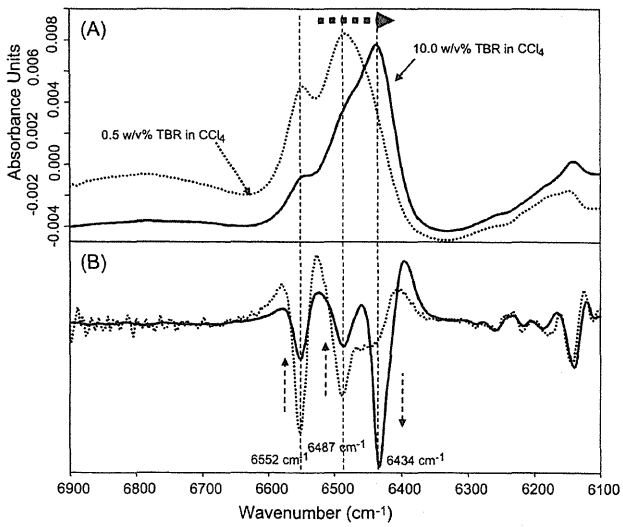

Fig. 4. NIR spectra obtained from the two TBR carbon tetrachloride (CCl_4) solutions. (A) Base line correlated spectra and (B) second derivative spectra.

Table 1
Wavenumbers of TBR (tulobuterol).

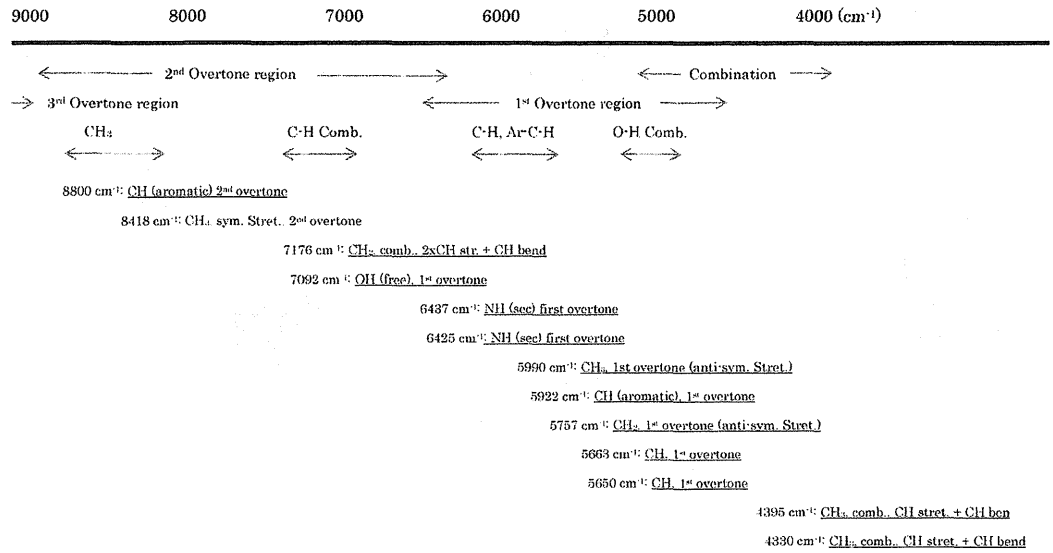

(w/v) solution, the two characteristic absorptions at 6552 cm^{-1} and 6487 cm^{-1} and the shoulder-like weak absorption at 6434 cm^{-1} were observed. In the spectra of 10.0% (w/v), the intensities of the absorptions at 6551 cm^{-1} and 6487 cm^{-1} were reduced, depending on the TBR concentration. Conversely, the intensity of the absorption at 6432 cm^{-1} increased depending on the TBR concentration. It was reported that a first overtone of secondary amine obtained from a dilute CCl_4 solution of butyl amine was observed at 6530 cm^{-1} [16]. A stretching of a secondary amine of each molecule of butyl amine would not be affected by an inter-molecular force from near molecules in a dilute solution. In addition, several examples of first overtone of N-H for a secondary amine (R-NH-R) in CCl_4 were reported from 6471 cm^{-1} to 6844 cm^{-1} [16]. The absorption at 6552 cm^{-1} observed in the present study is included in the reported wavenumber range based on the functional group. The positions of the three second derivative peaks obtained from crystalline TBR were observed at 10 cm^{-1} or 100 cm^{-1} lower peak positions compared to the corresponding peak positions obtained from the TBR CCl_4 solution.

Fig. 5 shows the time-course of peak intensities during the re-crystallization process after the melting of the TBR crystals. The spectra which were obtained from the samples in the early stage (less than 1 h), middle stage (from 1 h to 3 h), later stage (from 3 h to 24 h) and final stage (after 24 h) of the re-crystallization process are shown in the figure. The spectra obtained from the sample which contained no lumps of crystals that could be confirmed visually (0–40 min after melting and cooling) represent the wide and round-top peaks.

In addition, the peak widths and the peak intensities were getting narrow and strong with the passage of time, and the shape of the top of the absorptions became similar to that of the TBR standard substance. Although the three sharp peaks in the second derivative spectrum were not observed on the spectrum obtained from the sample within 1 h after melting, these peaks appeared at 3 h and the intensities became strong with the passage of time.

During the measurement, white crystals from the colorless lumps of amorphous TBR were observed in the vial. The authors suspect that the intensity of a first overtone of N—H stretching was getting stronger with the passage of time because an orientation of TBR molecules was arranged by means of re-construction of the crystalline structure. The N—H functional group in TBR will form an inter-molecular hydrogen bonding network between neighbor TBR molecules. A first overtone of N—H stretching derived from hydrogen bonding-formed secondary amine in TBR crystals was shifted to lower wavenumbers compared to free N—H stretching.

Moreover, the intensity of the second derivative peak at 6508 cm^{-1} was stronger and reached its maximum in the later stage, and then the intensity became smaller in the final stage of measurement. (The spectrum is represented in the enlarged window in Fig. 5B.) The spectra which were obtained from amorphous TBR are not shown here, in order to represent the other spectra clearly (the characteristic absorbance was not observed in the spectrum obtained from amorphous TBR). The intensity of the second

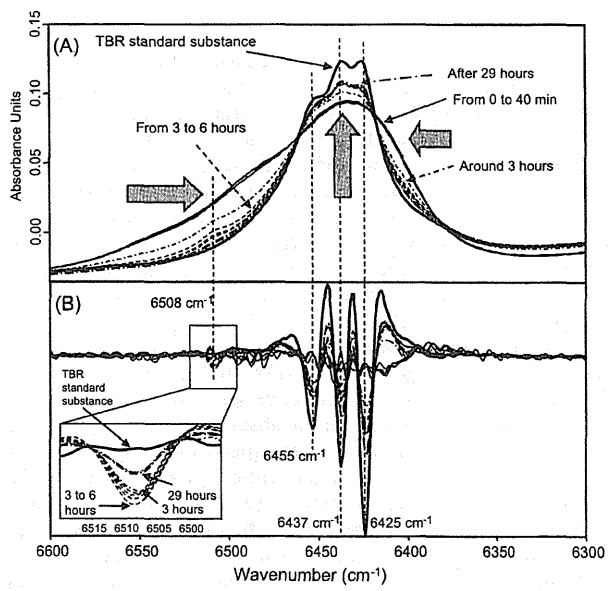

Fig. 5. Time-depending change of peak intensity and shape during the re-crystallization process of TBR. (A) Base line correlated spectra and (B) second derivative spectra.

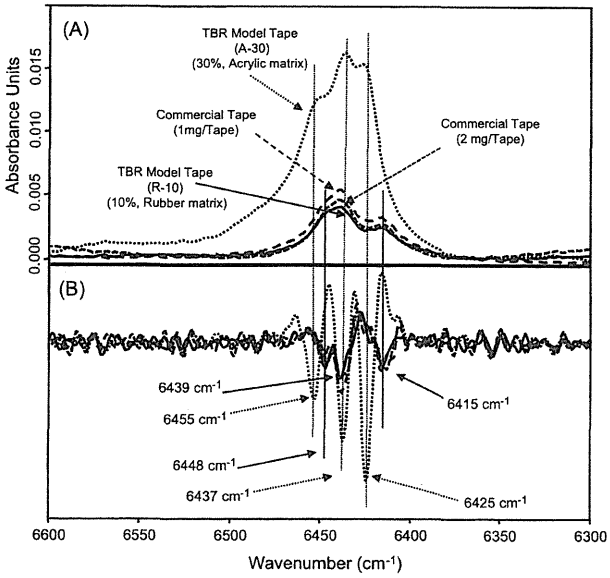

Fig. 6. NIR spectra obtained from the commercial tapes (1 mg/tape and 2 mg/tape) and the model tapes (A-30 and R-10). (A) Base line correlated spectra and (B) second derivative spectra.

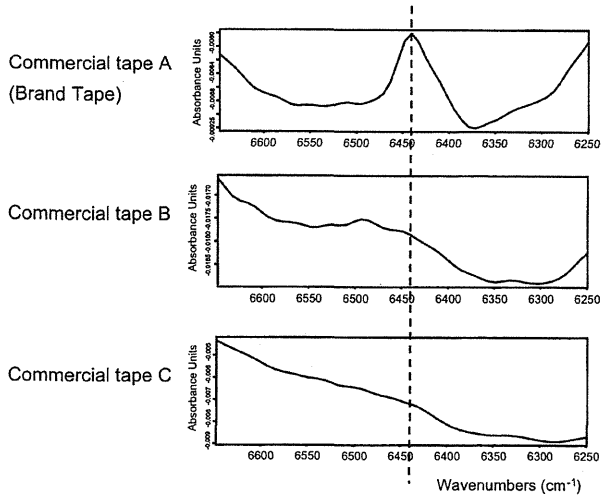

Fig. 7. NIR spectra obtained from the three kinds of commercial tapes (brand and other two commercial products).

derivative peak observed after 3 h at 6508 cm^{-1} increased at 6 h, but its intensity after 29 h was decreased. The intensity of that peak obtained from pure TBR disappeared.

The melting point of the small lumps of crystals in the early stage of re-crystallization was 82.6 °C (measured by differential scanning calorimetry). The measured melting point was the same as the melting point of a polymorph of TBR (a less stable Form 2) [17]. The melting point of the crystals in the final stage of re-crystallization was 90.4 °C, and that temperature is the same as the melting point of the pure TBR used as the standard substance for this study (a stable Form 1). This conclusion would support our experimental results and also suggest that the crystalline form of TBR would be transformed from amorphous to Form 1 via Form 2. The authors believe that the absorption at 6508 cm^{-1} would be characteristically detected in Form 2, and then it would disappear when the crystals transform to Form 1.

3.3. Detection of TBR crystals in the commercial tapes

The NIR spectra obtained from the commercial tapes are shown in Fig. 6. The N—H overlapped absorption from 6500 cm^{-1} to 6350 cm^{-1} was observed. The narrow broken line and the wide broken line represent the spectra obtained from the 2 mg-tape and 1 mg-tape, respectively. The peak intensities from both tapes are almost the same, because several different TBR contents of the tapes were made by cutting several different sizes from one large sheet (i.e., from one batch). The dotted line and the solid line represent the spectra obtained from the model tapes A-30 and R-10, respectively. The three peak positions of the second derivative spectra of the two types of commercial tape correspond to R-10 but not with A-30.

A comparison of the growth process of TBR crystals in two types of matrix measured by MLRSM was reported [12]. Although further study would be necessary to determine the details of the differences in the peak position between two types of matrix, an interaction such as hydrogen-bonding networks between the TBR crystal and each matrix would differ, and this difference may affect the peak position derived from the N—H first overtone.

In the present study, the detection of TBR crystals without removal of a liner that protects the adhesive side of the tape was possible by conducting transmittance-reflectance NIR measurements. Other commercial tapes which are used for the same clinical purpose but distributed by different manufacturers were also measured. Fig. 7 shows the NIR spectra obtained from these commercial tapes. The top of the three spectra represents the spectrum obtained from the brand product. The NIR spectra obtained from the other commercial tapes (which were from two different manufacturers) are also shown in the figure and no characteristic absorbance from 6500 cm^{-1} to 6350 cm^{-1} was observed. These results suggest that only the brand tape contains crystalline TBR in a matrix.

3.4. Time-dependent changes in the distribution of crystalline TBR in the model tapes

The absorbance intensities at 6340 cm^{-1} on days 3, 10, 17, 30, 42, 49 and 63 after the preparation were examined. Fig. 8(A) shows each NIR spectrum. The intensities on day 3 were almost the same as a fringe level, but they were significantly increased after day 10. After day 42, the intensities of absorbance reached a plateau. These results suggest that the crystallization term of TBR of this model tape is from 30 days to 40 days after the preparation. The correlation between absorption intensities and the elapsed days is shown in Fig. 8(B). The model tapes No. 1 to No. 3 were cut from one large sheet of the model tape. The relative intensities represent the ratio of the average intensity of three measurements of each model tape to that of a reference model tape which had been stored for about 6 months. Model tape No. 1 demonstrated strong intensities throughout the measurement term compared to the other tapes. The spot of NIR light is approximately 15 mm in dia., and the model tapes are each 36 mm in dia. Therefore, the authors used the average intensity obtained from three different measurement areas to cover the entire areas of the model tapes for calculation. This means that the crystallinity of TBR in each tape (each piece) would differ, and suggests that heterogeneity of distribution of TBR crystals would occur in the large sheet of model tape. The results suggest that NIRS is applicable for non-destructive quantitative predictions for an end-point of a crystallization process, and/or at a development stage.

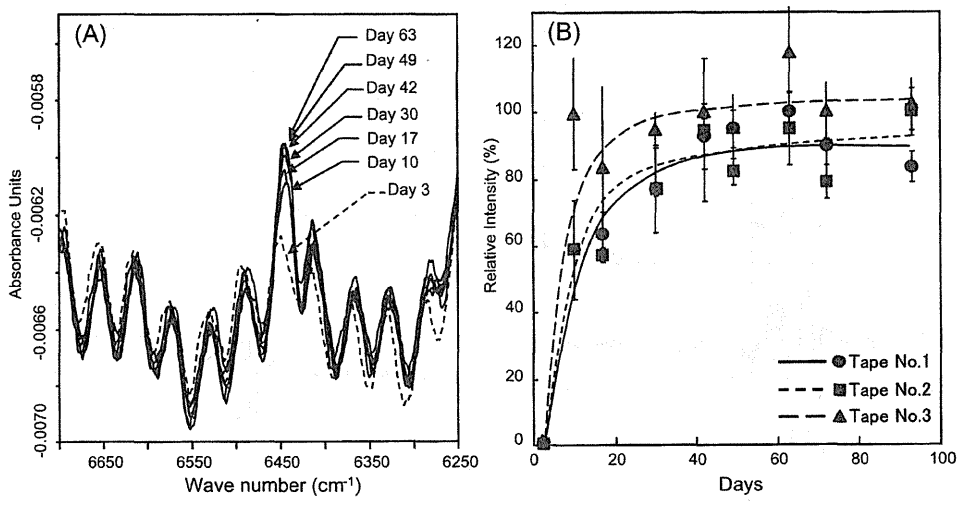

Fig. 8. (A) and (B) The time-course of peak intensities during the re-crystallization process after the melting of the TBR crystals, from day 3 to day 63 after the melting.

3.5. Chemical imaging of TBR crystals in matrix and time-course observations

Fig. 9 provides the NIR chemical images of the matrix of a model tape (R-10) and the corresponding area of the micro-photograph. The distribution of strong intensities based on a first overtone of secondary amine corresponded to the distribution of crystalline TBR which is observed in the micro-photograph.

Fig. 10 represents the NIR chemical images of the model tape (R-10) on days 2, 17, 23 and 37 in a 3-mm × 3-mm area after the preparation. Although lumps of TBR crystals that were detected using NIRI were not observed in the model tape 2 days after the preparation, two spots which are the origin of the lumps of TBR crystals were identified on day 17. These spots became larger with the passage of time. A total of nine lumps of TBR crystals were observed in this measurement area on day 37. Thus, a time-dependent aspect of crystallization was observed.

The authors also observed a crystal lump formation process in a rubber matrix, using MLRSM [12]. The results showed that TBR crystals formed many small lumps, and these lumps grew independently in the matrices of the model tapes. The results of the present study support those observations.

The combination of the visible identification of crystals in a matrix and chemical information based on NIR spectrometry using the absorption from 6500 cm^{-1} to 6350 cm^{-1} of crystalline TBR offers a highly specific measurement approach.

3.6. Rapid measurement of TBR crystals distribution in the entire area of a transdermal tape by microscopic mapping

The authors used macroscopic mapping to measurements of four pieces of the model tapes obtained from one batch was performed. A heterogeneous distribution of TBR crystals was observed in the certain tapes (Fig. 11). Notably, only one lump of crystals was found in the tape No. 1. However, lumps of crystals were distributed over approximately a half of the area of the matrix of the tape No. 4. According to the chemical maps of lumps of TBR crystals in the tapes, single lumps of crystals and small groups of several lumps of crystals were observed. One tape contained numerous lumps of TBR crystals that looked like a mountain chain, based on a rough image with 3-mm spatial resolution. These macroscopic maps were all obtained using the same intensity range. Thus, not only a distribution of TBR crystals but also a rough quantity of it TBR crystals can be estimated.

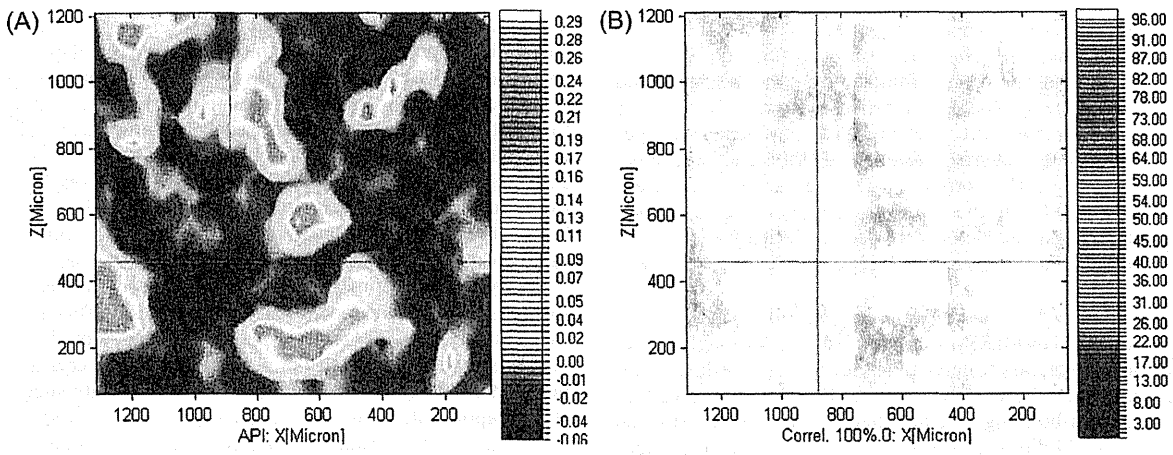

Fig. 9. NIR chemical image (A) and micro-photograph (B) of an R-10 model tape.

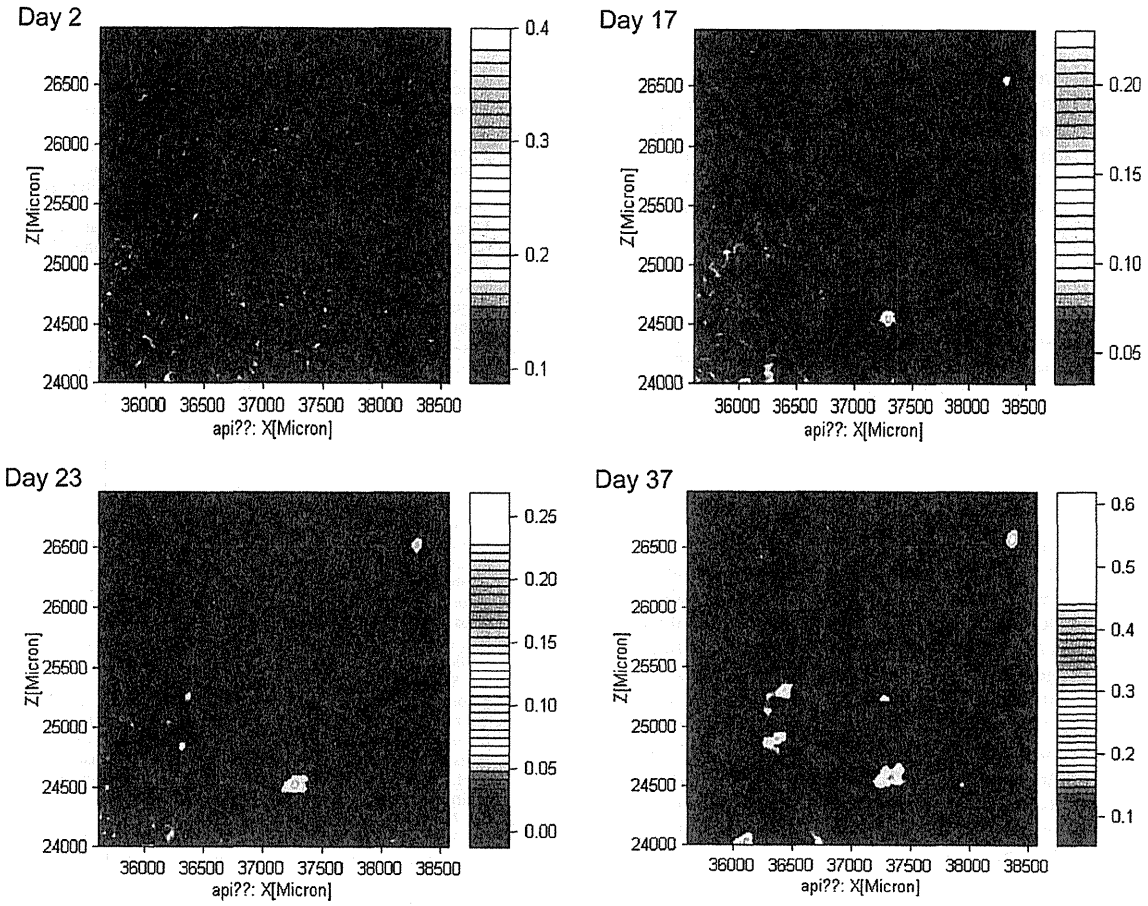

Fig. 10. Generation of TBR crystals in the model tape.

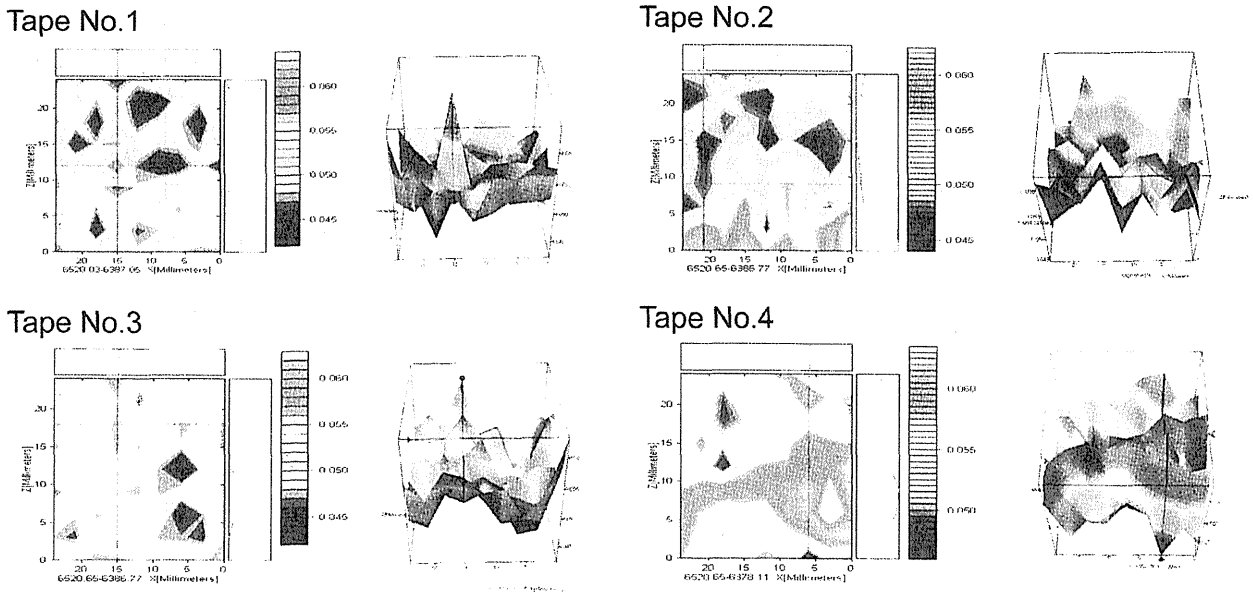

Fig. 11. NIR macroscopic maps of four commercial tapes obtained from the same batch.

Heterogeneity of the distribution and contents of TBR crystals in these model tapes was revealed by this approach, even though the model tapes were obtained from the same batch. If a heterogeneous distribution of TBR crystals will occur in each commercial tape, the pharmacological effects of the tapes may differ. The NIR spectroscopic and imaging techniques described herein will be useful to evaluate the homogeneity of TBR crystals in a matrix at the pharmaceutical development stage and/or in quality-control procedures.

4. Conclusion

The authors developed a method for determining the characteristics of TBR crystals in TDDS tapes using transmittance-reflectance NIR measurements. This method could be useful for quality evaluation for TBR TDDS tapes that have a crystal reservoir system. It is difficult to observe TBR crystals in a matrix through a supporting board and/or a liner in commercial tapes. Therefore, our method will contribute to the identification of TBR crystals in tapes which are in storage and/or on the market.

In addition, time-course measurements based on the characteristic absorption of crystalline TBR will also provide useful information for the estimation of an end-point of a crystallization process at a development stage, and for studies of crystallization mechanisms of an API in a matrix. The macroscopic mapping technique is advantageous for rapid analyses of the distribution of crystalline TBR, although only rough maps will be obtained. The authors obtained NIR measurements using a wavenumber range from 8000 cm^{-1} to 4000 cm^{-1}. But if the authors use a narrower wavenumber range which include the characteristic absorbance of a crystalline API to acquire a chemical maps, the authors would know a distribution of crystalline API in a matrix within a few minutes. A near infrared spectroscopy and imaging technique is useful as a non-destructive evaluation tool to secure the quality of TDDS pharmaceuticals.

Acknowledgements

This study was supported in part by a research grant from the Ministry of Health, Labour and Welfare of Japan (H20-iyaku-ippan-004).

The authors thank Dr. Yukio Aso and Dr. Tamaki Miyazaki, Division of Drugs, National Institute of Health Sciences, for their kind cooperation regarding the polymorphs of TBR and the differential scanning calorimetry measurements. The authors thank Mr. Daisuke Sasakura, Mr. Tomoyuki Matsuara and Mr. Tsuyoshi Miura, Bruker Optics K.K., for their kind assistance in the measurement of TDDS tapes using the NIR microscopic imaging system.

References

[1] T. Uematsu, M. Nakano, K. Kosuge, M. Kanamaru, M. Nakashima, The pharmacokinetics of the beta 2-adrenocepter agonist, tulobuterol given transdermally and by inhalation, Eur. J. Clin. Pharmacol. 44 (1993) 361–364.

[2] T. Horiguchi, R. Kondo, J. Miyazaki, K. Fukumoto, H. Torigoe, Clinical evaluation of a transdermal therapeutic system of β2-agonist tulobuterol in patients with mild or moderate persistent bronchial asthma, Arzneinittelforschung 54 (2004) 280–285.

[3] Y. Iikura, H. Uchiyama, K. Akimoto, M. Ebisawa, N. Sakaguchi, T. Tsubaki, H. Ishizu, H. Kabayama, K. Yagi, K. Miura, Pharmacokinetics and pharmacodynamics of the tulobuterol patch, HN-078, in childhood asthma, Ann. Allergy Asthma Immunol. 74 (1995) 147–151.

[4] T. Horiguchi, R. Kondo, J. Miyazaki, H. Torigoe, S. Tachikawa, Clinical evaluation of tulobuterol patch in patients with mild or moderate persistent bronchial asthma—effects of long-term treatment on airway inflammation and hypersensitivity, Nihon Kokyuki Gakkai Zasshi 42 (2004) 132–137 (in Japanese).

[5] H. Kato, O. Nagata, M. Yamazaki, T. Suzuki, Y. Nakano, Development of transdermal formulation of tulobuterol for the treatment of bronchial asthma, Yakugaku Zasshi 122 (2002) 57–69 (in Japanese).

[6] M. Otsuka, F. Kato, Y. Matsuda, Comparative evaluation of the degree of indomethacin crystallinity by chemoinfometrical Fourier-transformed near-infrared spectroscopy and conventional powder X-ray diffractometry, AAPS PharmSci. 2 (1) (2000) E9.

[7] M. Otsuka, F. Kato, Y. Matsuda, Determination of indomethacin polymorphic contents by chemometric near-infrared spectroscopy and conventional powder X-ray, Analyst 126 (2001) 1578–1582.

[8] A. Gambás, I. Antai, P. Szabó-Révész, S. Marton, I. Erõs, Quantitative determination of crystallinity of alpha-lactose monohydrate by near infrared spectroscopy (NIRS), Int. J. Pharm. 256 (2003) 25–32.

[9] S.J. Bai, M. Rani, R. Suryanarayanan, J.F. Carpenter, R. Nayar, M.C. Manning, Quantification of glycine crystallinity by near-infrared (NIR) spectroscopy, J. Pharm. Sci. 93 (2004) 2439–2447.

[10] M. Savolainen, A. Heinz, C. Strachan, K.C. Gordon, J. Yliruusi, T. Rades, N. Sandler, Screening for differences in the amorphous state of indomethacin using multivariate visualization, Eur. J. Pharm. Sci. 30 (2007) 113–123.

[11] M. Allesø, S. Velaga, A. Alhalaweh, C. Cornett, M.A. Rasmussen, F. van den Berg, H.L. de Diege, J. Rantanen, Near-infrared spectroscopy for cocrystal screening. A comparative study with Raman spectroscopy, Anal. Chem. 80 (2008) 7755–7764.

[12] T.R. De Beer, P. Vercruysse, A. Burggraeve, T. Quinten, J. Ouyang, X. Zhang, C. Vervaet, J.P. Remon, W.R. Baeyens, In-line and real-time process monitoring of a freeze drying process using Raman and NIR spectroscopy as complementary process analytical technology (PAT) tools, J. Pharm. Sci. 98 (2009) 3430–3446.

[13] B. Connolly, T.W. Patapoff, Y.J. Wang, J.M. Moore, T.J. Kamerzell, Vibrational spectroscopy and chemomatrics to characterize and quantitate trehalose crystallization, Anal. Biochem. 399 (2010) 48–57.

[14] T. Sakamoto, T. Matsubara, D. Sasakura, Y. Takada, Y. Fujimaki, K. Aida, T. Miura, T. Terahara, N. Higo, T. Kawanishi, Y. Hiyama, Chemical mapping of tulobuterol in transdermal tapes using microscopic laser Raman spectroscopy, Pharmazie 64 (2009) 166–171.

[15] T. Sakamoto, A. Portieri, P.F. Taday, Y. Takada, D. Sasakura, K. Aida, T. Matsubara, T. Miura, T. Terahara, D.D. Arnone, T. Kawanishi, Y. Hiyama, Detection of tulobuterol crystal in transdermal patches using terahertz pulsed spectroscopy and imaging, Pharmazie 64 (2009) 361–365.

[16] J. Workman Jr., L. Weyer, Practical Guide to Interpretive Near-Infrared Spectroscopy, CRC Press, Florida, 2007.

[17] M.R. Caira, S.A. Bourne, C.L. Oliver, Thermal and structural characterization of two polymorphs of the bronchodilator tulobuterol, J. Therm. Anal. Calorim. 77 (2004) 597–605.

International Journal of Pharmaceutics 441 (2013) 135–145

Contents lists available at SciVerse ScienceDirect

International Journal of Pharmaceutics

journal homepage: www.elsevier.com/locate/ijpharm

Detection of component segregation in granules manufactured by high shear granulation with over-granulation conditions using near-infrared chemical imaging

Tatsuo Koide[a,*], Takuya Nagato[b], Yoshiyuki Kanou[b], Kou Matsui[b], Susumu Natsuyama[b], Toru Kawanishi[a], Yukio Hiyama[a]

[a] Division of Drugs, National Institute of Health Sciences, 1-18-1 Kamiyoga, Setagaya-ku, Tokyo 158-8501, Japan
[b] Powrex Corporation, Osaka Powder Technology Center, 8-121-1 Kitaitmi, Itami 664-0831, Japan

ARTICLE INFO

Article history:
Received 2 August 2012
Received in revised form 7 November 2012
Accepted 5 December 2012
Available online 12 December 2012

Keywords:
Image analysis
Near-infrared spectroscopy
High shear granulation
Segregation

ABSTRACT

The objective of this study was to evaluate the high shear granulation process using near-infrared (NIR) chemical imaging technique and to make the findings available for pharmaceutical development. We prepared granules and tablets made under appropriate- and over-granulation conditions with high shear granulation and observed these granules and tablets using NIR chemical imaging system. We found an interesting phenomenon: lactose agglomeration and segregation of ingredients occurred in experimental tablets when over-granulation conditions, including greater impeller rotation speeds and longer granulation times, were employed. Granules prepared using over-granulation conditions were larger and had progressed to the consolidation stage; segregation between ethenzamide and lactose occurred within larger granules. The segregation observed here is not detectable using conventional analytical technologies such as high pressure liquid chromatography (HPLC) because the content of the granules remained uniform despite the segregation. Therefore, granule visualization using NIR chemical imaging is an effective method for investigating and evaluating the granulation process.

1. Introduction

In the pharmaceutical manufacturing of solid dosage forms, the major aim of the granulation process is to produce granules with attributes that are beneficial for manufacturing, such as flowability, and contribute to high quality, such as homogeneity. Flowability and homogeneity depend on the conditions used during granulation. Despite the best efforts of manufacturers, the granulation process is sometimes poorly controlled and is characterized by quality control problems such as delay in dissolution. Granulation is one of the most critical processes in the manufacture of pharmaceutical solid dosage forms. Establishment of reliable manufacturing processes requires an understanding of the granulation process and identification and application of the critical factors that determine granulation quality. The ICH Q8 guidelines emphasize the adoption of quality by design (QbD) in the development of pharmaceutical products; this is a systematic approach based on scientific principles. Information gained from pharmaceutical development studies provides scientific knowledge to support the optimization of manufacturing processes, which in turn promotes quality in pharmaceutical products. In order to sufficiently understand the granulation process and produce higher quality products, highly accurate evaluation methods are necessary. Near-infrared (NIR) chemical imaging is one of the best methods for analyzing granulation because it can characterize heterogeneous solid dosage forms at a micron scale along with spatial and chemical information. In addition, this technique is rapid and nondestructive and requires a simpler sample preparation than that required for other chemical mapping methods. NIR chemical imaging has revealed more chemical information about solid dosage forms, such as tablets, capsules, powders, and freeze-dried product than that revealed by HPLC or other conventional analytical technologies (El-hagrasy et al., 2001; Jovanovic et al., 2006; Lewis et al., 2004; Linda et al., 2007; Lyon et al., 2002; Shah et al., 2007). This imaging method has been used to identify the causes of problems that occur during blending, granulating, and tableting (Clarke et al., 2001; Clarke, 2004; Hammond and Clarke, 2002). In addition, NIR has been successfully used to assess the quality of pharmaceutical products purchased on the Internet and to screen for counterfeit drugs in the US (Dubois et al., 2007;

* Corresponding author. Tel.: +81 03 3700 8694; fax: +81 03 3707 6950.
E-mail address: koide@nihs.go.jp (T. Koide).

0378-5173/$ – see front matter © 2012 Elsevier B.V. All rights reserved.
http://dx.doi.org/10.1016/j.ijpharm.2012.12.005

Veronin and Youran, 2004; Westenberger et al., 2005). Thus, previous research has shown that NIR chemical imaging is useful for various types of pharmaceutical analysis. Therefore, the method has attracted much attention for potential uses in process analysis, quality control, and product evaluation in pharmaceutical manufacturing.

Several granulation methods are presently used in pharmaceutical manufacturing. Wet granulation methods are now more widely used in the manufacturing process than dry granulation and direct compression methods. In the Japanese pharmaceutical industry, wet granulation methods are used in more than 70% of all manufacturing runs (Sunada et al., 2003). The mechanism of high shear granulation, which is one of the commonly used wet granulation methods, has been the subject of several investigations with respect to its mechanisms (Iveson et al., 2001; Saleh et al., 2005; Vonk et al., 1997). These studies have determined that the process of high shear granulation involves 3 key stages: wetting and nucleation, consolidation and growth, and breakage and attrition. Granules made under different formulation and granulation conditions have different properties (Benali et al., 2009; Vemavarapu et al., 2009). The process of high shear granulation is not well-understood due to its high complexity. A better understanding of this mechanism could lead to applications that would enhance the manufacture of pharmaceuticals.

In this study, we systematically investigated high shear granulation. The granulation conditions were selected based on previously reported data (Tanino et al., 2006) to produce both appropriate-granulation and over-granulation. We used NIR chemical imaging to observe differences between good and poor quality granules and tablets made under differing granulation conditions. Additionally, the feasibility of using NIR chemical imaging to describe granule properties and to evaluate the pharmaceutical development process is discussed.

2. Materials and methods

2.1. Materials

Ethenzamide, which was the active ingredient, was provided by Shionogi & Co., Ltd. (Osaka, Japan). Cornstarch, 200 mesh lactose monohydrate, and methylcellulose were purchased from Nihon Shokuhin Kako Co., Ltd. (Tokyo, Japan), DMV International (Veghel, The Netherlands) and Shin-Etsu Chemical Co., Ltd. (Tokyo, Japan), respectively. The other reagents used in this experiment were of laboratory grade.

2.2. Methods

2.2.1. High shear granulation process

The granules were manufactured on a scale of 5 kg. Four compounds (ethenzamide, 70% (w/w); cornstarch, 7.9%; lactose, 18.6%; and methyl cellulose, 3.5%) were mixed with an impeller rotation speed of 240 rpm for 2 min, then supplemented with water (1100 g) and granulated using a VG-25 high shear granulator (Powrex Corporation, Itami, Japan). The chopper rotation speed was 3000 rpm and the water addition rate was about 27.5 g/s. The granules were made using different granulation times (3, 5, and 10 min) and impeller speeds (40, 120, and 200 rpm). The coarse milling of the wet granules was performed using a Comill QC-197S screening mill (Powrex Corporation) with an open mesh screen of 4.75 mm diameter and an impeller speed of 2400 rpm. The granulated wet mass was dried with a compartment dryer (Yamato Scientific Co., Ltd., Tokyo, Japan) at 60 °C for 12 h. The final water content of the granules was less than 1.0% (loss on drying test).

2.2.2. Particle size analysis

The particle size of the material components was measured using a particle-viewer laser diffraction particle size analyzer (Powrex Corporation) with a 632.8 nm He–Ne laser beam. From these results, a particle size distribution curve was drawn and the diameters (D_{10}, D_{50}, and D_{90}) were calculated.

The size of granules produced by high shear granulation was measured by the sieve analysis method using an Iida testing sieve (Iida Manufacturing Co., Ltd., Tokyo, Japan). The particle size of the granules was evaluated using an 8.6, 16, 22, 30, 50, 83, 140, or 200 mesh sieve. The granule size distributions were calculated by determining the ratios of the residual weight of the granules on each sieve to the granule weight before sieving. On the basis of these results, a particle size distribution curve was drawn and the median diameter (D_{50}) was calculated.

2.2.3. Preparation of samples for measurement

The granule samples were obtained from various areas in the ball of the granulator. The granules were compressed by hand into experimental tablets using 300 mg of granules and 2 kN pressure and then analyzed using an NIR imaging system. For producing a spectral library of the components, pure reference wafers were prepared in the same manner as the samples.

The sieved granules were classified into 3 categories: large-size granules that were left on the 8.6 and 16 mesh sieves (>1000 μm), medium-size granules left on the 22 and 30 mesh sieves (500–1000 μm), and small-size granules passed though the 30 mesh sieves (<500 μm). Size-classified granules were then compressed by hand into experimental tablets using 300 mg of granules and 2 kN pressure and measured using an NIR imaging system to investigate the relationship between granule size and chemical image. Size-classified granules were also analyzed using a UV quantitative assay.

The granules for single granule measurement by NIR chemical imaging were embedded in wafers of anhydrous caffeine. The embedded granules were then trimmed by EM trim (Leica Microsystems, Wetzlar, Germany) and sectioned to observe the interior of each granule. The distinct NIR spectrum of anhydrous caffeine allowed for easy removal of this substance from the NIR chemical images using chemometrics.

2.2.4. NIR chemical imaging

The Spotlight 350 (Perkin Elmer, Waltham, MA), a chemical imaging system equipped with a liquid nitrogen-cooled 16 × 1 mercury cadmium telluride (MCT) linear array detector, and Spotlight data acquisition software (Version 1.0), were used to collect NIR spectra of the samples. Each spectrum came from a square pixel of 25 μm × 25 μm. The background scan was recorded at 16 cm^{-1} spectral resolution with 90 scans using a gold mirror as the reflectance standard, and the sample scan was recorded at 16 cm^{-1} spectral resolution with 4 scans across the wavelength 7600–3800 cm^{-1}.

An area of approximately 4.5 mm × 4.5 mm (approximately 30,000 pixels) on the surface of each experimental tablet was measured using the NIR chemical imaging system. Approximately 30 min were required to obtain the measurements for each tablet. Reference wafers of pure components were scanned in the same manner as the samples to create a reflectance spectral library of the components.

Analysis of the data was conducted using Isys chemical imaging software (version 4.0; Malvern Instruments, Ltd., Worcestershire, UK). The reflectance spectra were converted to absorbance spectra using the inverse common logarithm to convert to $\log(1/R)$; spectral data were normalized using the standard normal variate (SNV) method (Barnes et al., 1989) to remove any offsets due to physical variations such as path length. The normalized spectral data for

Table 1
Particle Sizes of the ingredients.

	D_{10} (μm)	D_{50} (μm)	D_{90} (μm)
Ethenzamide	8.3	21.5	129.9
Lactose	9.0	33.0	64.7
Cornstarch	9.6	17.4	27.4
Methylcellulose	26.6	64.0	128.5

the granules and tablets were used to generate chemical images using the partial least square type 2 (PLS2) multivariate analysis method (Makein et al., 2008; Rosipal and Krämer, 2006) based on the spectral library of pure reference components. The PLS score was calculated as the degree of membership between the spectra of each pixel and pure component, when the ratio of the spectra of image pixels fitted to the spectra of pure components was taken as 1. In the NIR chemical image, the brighter areas (high PLS scores) represented a higher level of components, while the darker areas represented a lower level of components. In order to analyze different aspects of the NIR data, histograms were generated, placing the PLS score on the *X*-axis and the number of pixels on the *Y*-axis. The *X*-axis was divided into 100 areas between the maximum and minimum PLS scores.

2.2.5. Active pharmaceutical ingredient (API) quantitative assay of ethenzamide

Quantitative assay of ethenzamide in the granules was performed using UV–vis spectrophotometry. A 4–8 mg portion of granules (1 large-sized granule or several middle- and small-sized granules) from each size category was weighed out and dissolved in purified water. For the UV measurements, the concentration of dissolved granules in the water was 4–8 mg/100 mL. The absorbance of ethenzamide was measured at a wavelength of 290 nm using the UV-2450 spectrophotometer (Shimadzu Corp., Kyoto, Japan) with purified water as the blank. The path length of the sample cell was 1.0 cm. The content of ethenzamide in the granules was calculated using a reference-standard calibration curve.

3. Results

3.1. Particle-size analysis of ingredients

The particle sizes of the ingredients are shown in Table 1. The D_{10} and D_{50} values of ethenzamide, lactose, and cornstarch were similar, but the D_{90} of cornstarch (27.4 μm) was much smaller than that of ethenzamide (129.9 μm) or lactose (64.7 μm). This means that there were fewer large particles of cornstarch than ethenzamide or lactose. The D_{10} and D_{50} of methylcellulose were larger than those of the other ingredients, indicating that there were fewer small particles of methylcellulose than the other compounds.

Table 2
D_{50} (μm) of granule size.

Impeller speed (rpm)	3 min granulation (μm)	5 min granulation (μm)	10 min granulation (μm)
40	313	296	339
120	313	455	922
200	502	698	1439

3.2. NIR chemical imaging analysis of granulation conditions in experimental tablets

NIR chemical images of wafer of pre-mixture powder before granulation are shown in Fig. 1. Typical NIR chemical images of the experimental tablets manufactured using different impeller rotation speeds and granulation times are shown in Figs. 2–4. The distribution of the components in the tablets made from granulation using an impeller rotation speed of 40 rpm appeared homogenous (Fig. 2), similar to the images of the pre-mixture powder (Fig. 1). However, images of ethenzamide and lactose in the tablets made from granulation using an impeller rotation speed of 120 rpm for more than 5 min (Fig. 3) and at 200 rpm for 3, 5, and 10 min (Fig. 4) showed uneven distributions of components; lactose domains with a diameter of 50–200 μm became evident due to agglomeration (Figs. 3 and 4). In particular, the brighter domains in the images of the lactose with 120 and 200 rpm granulation for 10 min indicated extensive agglomeration. It is noteworthy that domains with extensive lactose agglomeration have significantly low PLS scores for ethenzamide. We observed that lactose distribution generally contrasted that of ethenzamide under these conditions. Unlike ethenzamide or lactose, cornstarch did not form large domains because of its small particle size in D_{90}. Images revealed scattering of particles. However, when greater rotation speeds and longer granulation times were employed, such as 200 rpm for 10 min (Fig. 4), the distributions of ethenzamide and cornstarch overlapped. Unlike the other compounds, no distinguishing characteristics were observed between the various images of methylcellulose (Figs. 2–4). The phenomena described above were observed in all experimental tablets (10 tablets analyzed per set of conditions) measured by the NIR chemical imaging system (data not shown).

3.3. Effects of granulation conditions on granule size

The granules sizes produced by different granulation conditions are shown in Table 2. The granules sizes produced using an impeller speed of 40 rpm for 3, 5, and 10 min and 120 rpm for 3 min were approximately 300 μm. The images of tablets made using these granulation conditions indicate homogeneity (Figs. 2 and 3). In

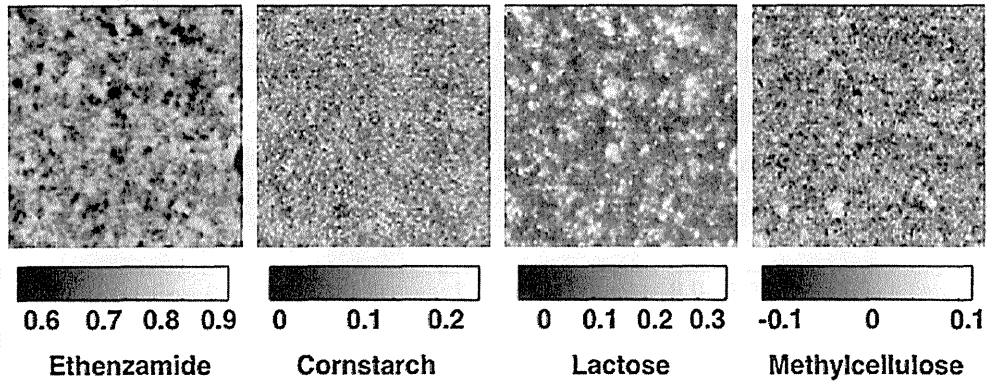

Fig. 1. NIR images of each of the 4 components of the pre-mixture wafer. For each of the 4 components, the PLS score bar is shown.

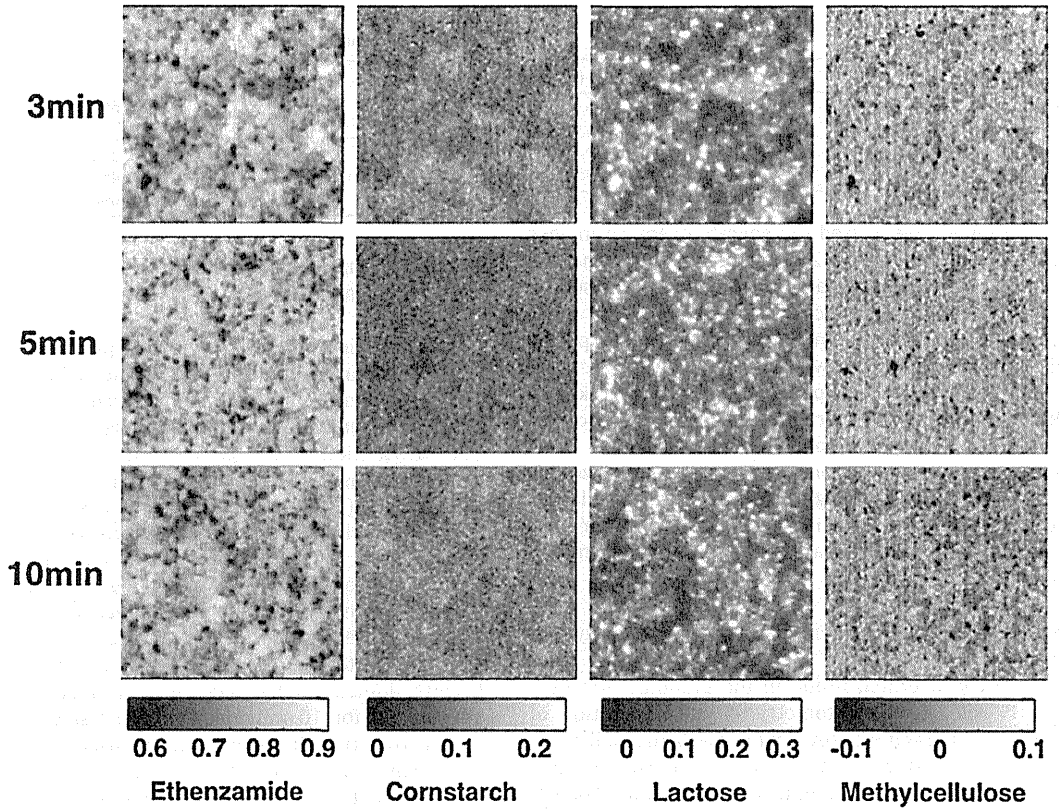

Fig. 2. NIR images of each of the 4 components of the experimental tablets made of granules produced using an impeller rotation speed of 40 rpm for 3, 5, or 10 min. For each of the 4 components, the PLS score bar is shown.

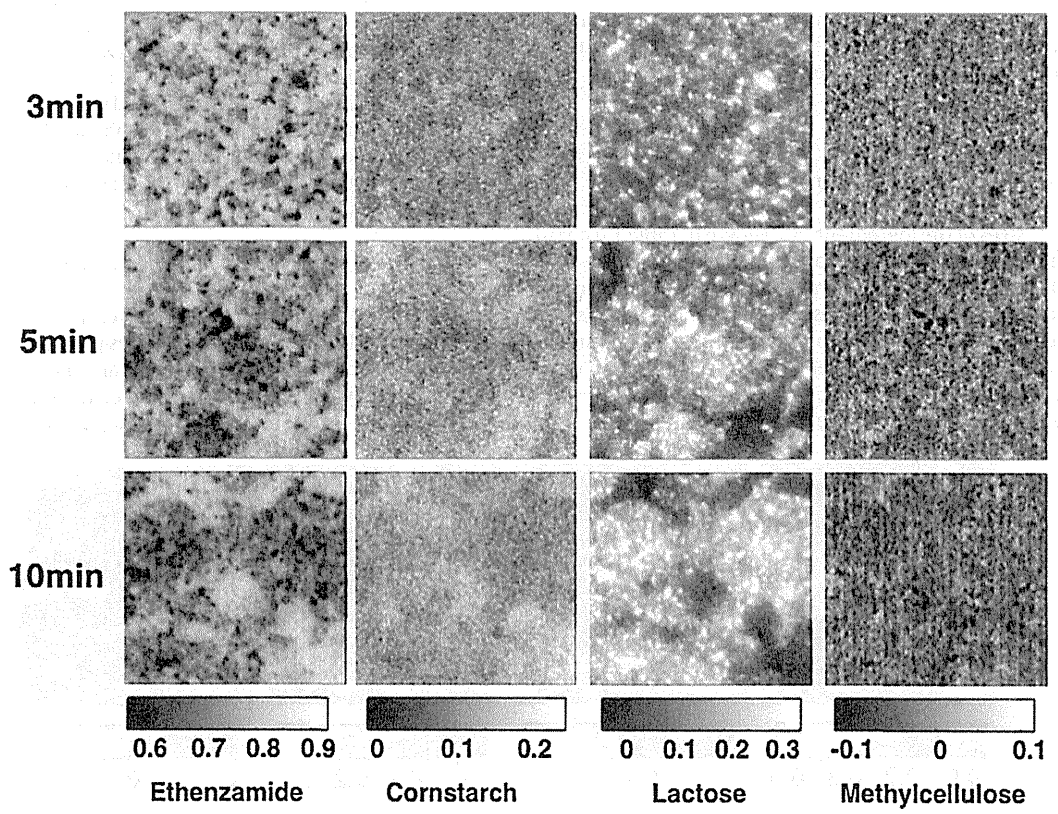

Fig. 3. NIR images of each of the 4 components in the experimental tablets made of granules produced using an impeller rotation speed of 120 rpm for 3, 5, or 10 min. For each of the 4 components, the PLS score bar is shown.

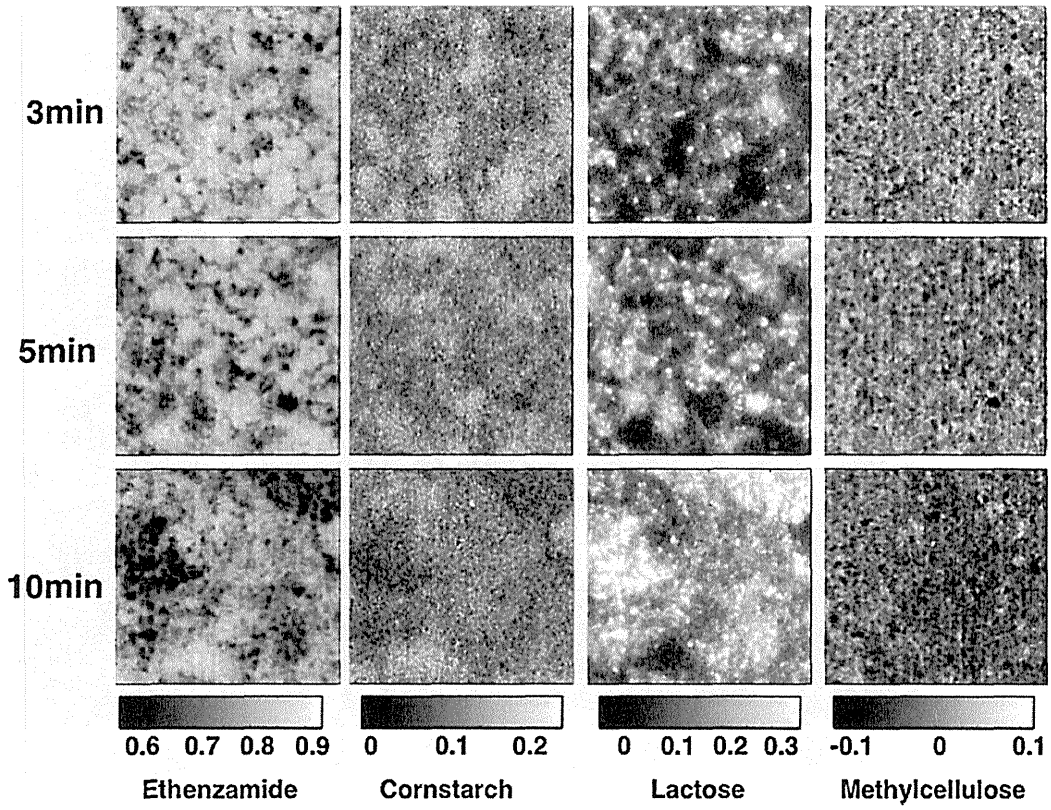

Fig. 4. NIR images of each of the 4 components in the experimental tablets made of granules produced using an impeller rotation speed of 200 rpm for 3, 5, or 10 min. For each of the 4 components, the PLS score bar is shown.

contrast, the granules made with an impeller rotation speed of 120 rpm for 5 min and 200 rpm for 3 and 5 min were larger, 455–698 μm (Table 2), with lactose agglomerations (Figs. 3 and 4). Furthermore, granulation performed at 120 or 200 rpm for 10 min led to excessive granulation, yielding D_{50} values of more than 900 μm (Table 2). Under these conditions, clear segregation of ethenzamide and lactose was revealed in the tablet images (Figs. 3 and 4).

Fig. 5 shows the particle size distribution of granules produced using an impeller speed of 40, 120 or 200 rpm and granulation time of 5 min. The number of larger granules increased with greater impeller speeds. When the impeller speed was increased from 40 to 200 rpm, the percentage of large-size granules (>1000 μm) increased from 6.0% to 33.0%, and that of small-size granules (<500 μm) decreased from 80.0% to 31.2%. In spite of the similar sizes, large-size granules produced at an impeller speed of 40 rpm were very fragile by feel and were not clearly consolidated compared to those produced at 200 rpm, which were hard and were well-consolidated. Overall, these results showed that granules produced using greater speeds and longer granulation times tended to be larger (Table 2 and Fig. 5) and more consolidated. With increased granule size and consolidation, lactose agglomeration and segregation were observed in tablet images (Figs. 3 and 4).

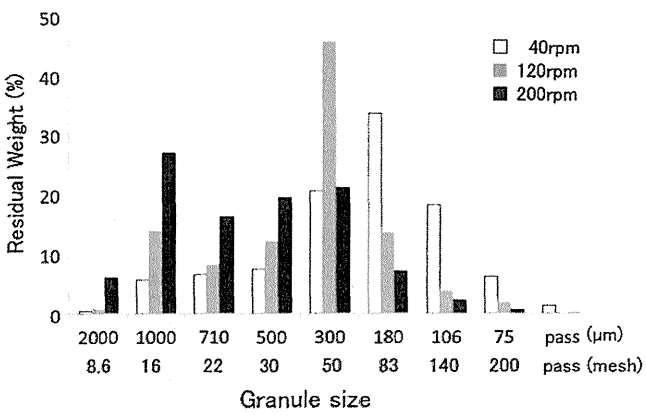

Fig. 5. Distribution of granule size using the sieving method.

3.4. Effects of granule size on component distribution

Images of tablets made of different sized granules are shown in Figs. 6 and 7. Tablets made of the large- and medium-size granules (granulation at 40 rpm for 5 min) showed slight agglomeration of lactose (Fig. 6). In contrast, the tablets made of small-size granules were homogeneous (Fig. 6). Tablets made of large- and medium-size granules (granulation at 200 rpm for 5 min) showed de-mixing and segregation; the tablets made of large-size granules showed particularly heavy segregation (Fig. 7). This result is similar to that observed for tablets with granules made under excessive granulation conditions, as shown in Figs. 3 and 4. In contrast, the tablets made of the small-size granules were homogenous.

To compare the distribution of the granule properties with respect to production method, histograms were created using the same data sets as used for the NIR chemical images. Figs. 8 and 9 show the histograms of the data sets used for the images in Figs. 6 and 7, respectively. A single peak, indicating homogeneous distribution, was observed in each ingredient histogram for the small-size granules. Broader peaks indicating a more

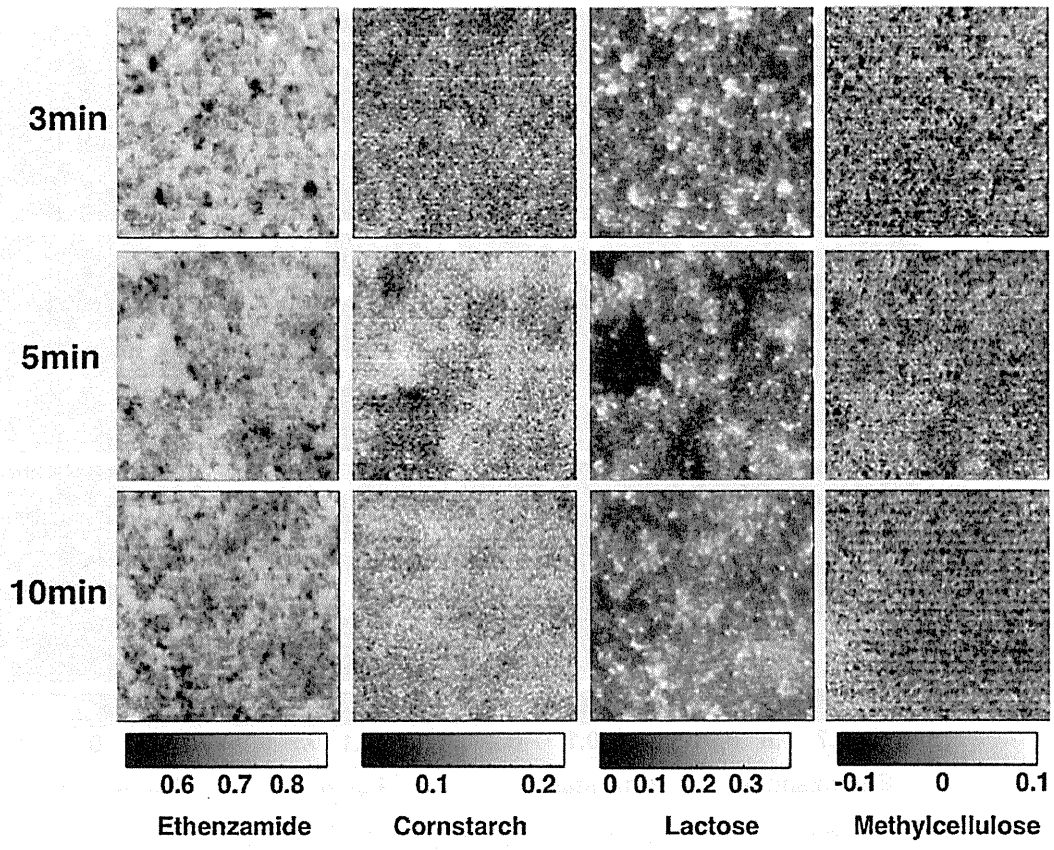

Fig. 6. NIR images of each of the 4 components in the experimental tablets made of size-classified granules produced using an impeller rotation speed of 40 rpm for 5 min. For each of the 4 components, the PLS score bar is shown.

inhomogeneous distribution were observed in the ethenzamide and lactose histograms of medium-size granules made under both low (40 rpm, Fig. 8) and high (200 rpm, Fig. 9) impeller speed. In the case of the large-size granules, single peaks appeared in the ethenzamide and lactose histograms made under a low impeller speed (Fig. 8), while two characteristic peaks indicating a high degree of inhomogeneity were apparent in the ethenzamide and lactose histograms made under a high impeller speed (Fig. 9). In the case of cornstarch, a broad peak was found only in the histogram of the tablet made of large-size granules under a high-speed condition. On the other hand, the methylcellulose histograms had a sharp peak under both conditions and did not show any significant changes correspondent with changes in the granule size or granulation conditions (data not shown). Based on these results from the images and histograms, the segregation occurred in the larger and more consolidated granules.

3.5. Single granule images

Typical chemical images of single granule produced under specific granulation conditions are shown in Fig. 10 (40 rpm, 5 min) and Fig. 11 (200 rpm, 5 min). The granules were trimmed to observe their interior (see Section 2). The granule produced under granulation conditions of 40 rpm for 5 min was homogenous (Fig. 10). However, significant segregation was observed in the interior section of the granule produced at 200 rpm for 5 min (Fig. 11). Clear segregation was observed between the ethenzamide on the upper portion and lactose on the lower portion of the granule (Fig. 11). The blue area around the granule in the images represents embedded caffeine. This segregation was found in most of the large-size granules made under granulation conditions of 200 rpm and 5 min but not under conditions of 40 rpm and 5 min.

3.6. Distribution of ethenzamide in granules

The content of ethenzamide in various-size granules was examined by quantitative assays using the UV method (Table 3). The ethenzamide content was approximately 70% under granulation conditions of 40 rpm and 200 rpm for 5 min. These values were close to the theoretical value (70%) for both granulation conditions even though NIR imaging indicated de-mixing and segregation of ethenzamide and lactose. This result showed that there was no substantial difference in ethenzamide content between the different granule sizes.

4. Discussion

Our observations in this study indicate that granule size increased with increasing speeds and times of high shear

Table 3
Contents of ethenzamide in the granules as measured by UV.

Impeller speed (rpm)	Size	Average of ethenzamide Content (%) ± SD (n = 3)
40	Large	70.6 ± 1.8
	Medium	69.9 ± 1.3
	Small	70.0 ± 0.2
200	Large	72.3 ± 0.6
	Medium	72.1 ± 1.6
	Small	72.5 ± 0.3

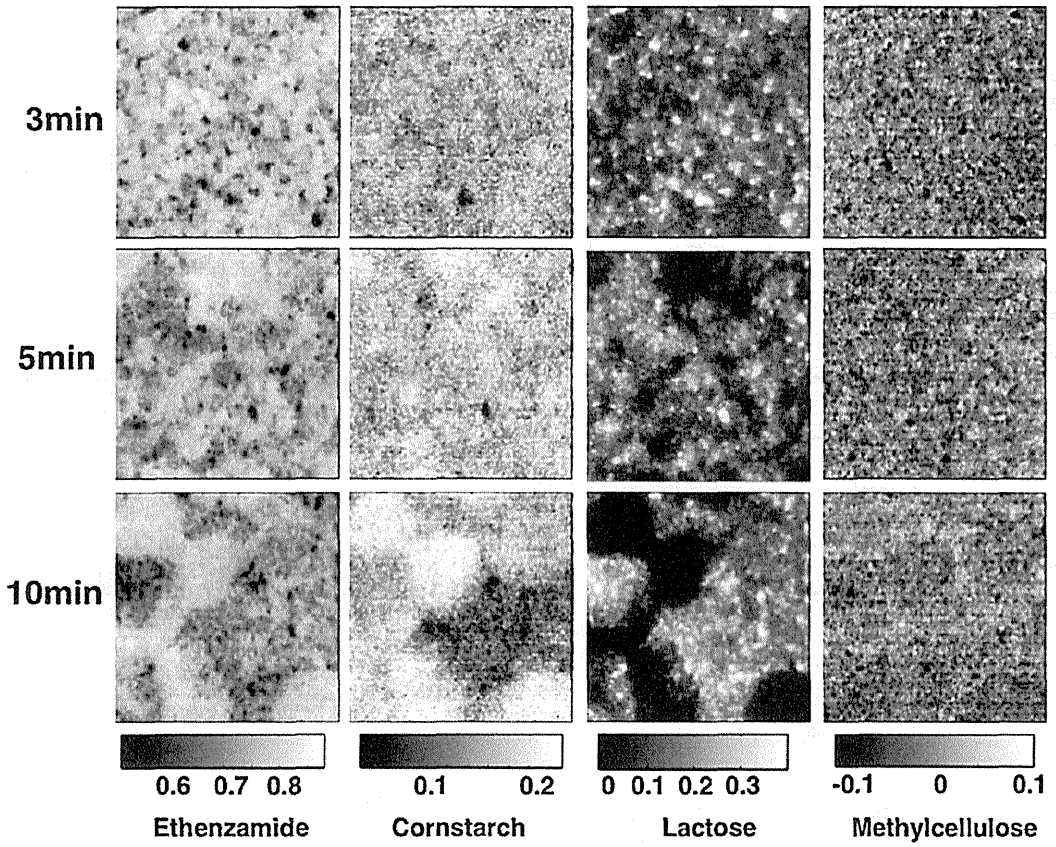

Fig. 7. NIR images of each of the 4 components in the experimental tablets made of size-classified granules produced using an impeller rotation speed of 200 rpm for 5 min. For each of the 4 components, the PLS score bar is shown.

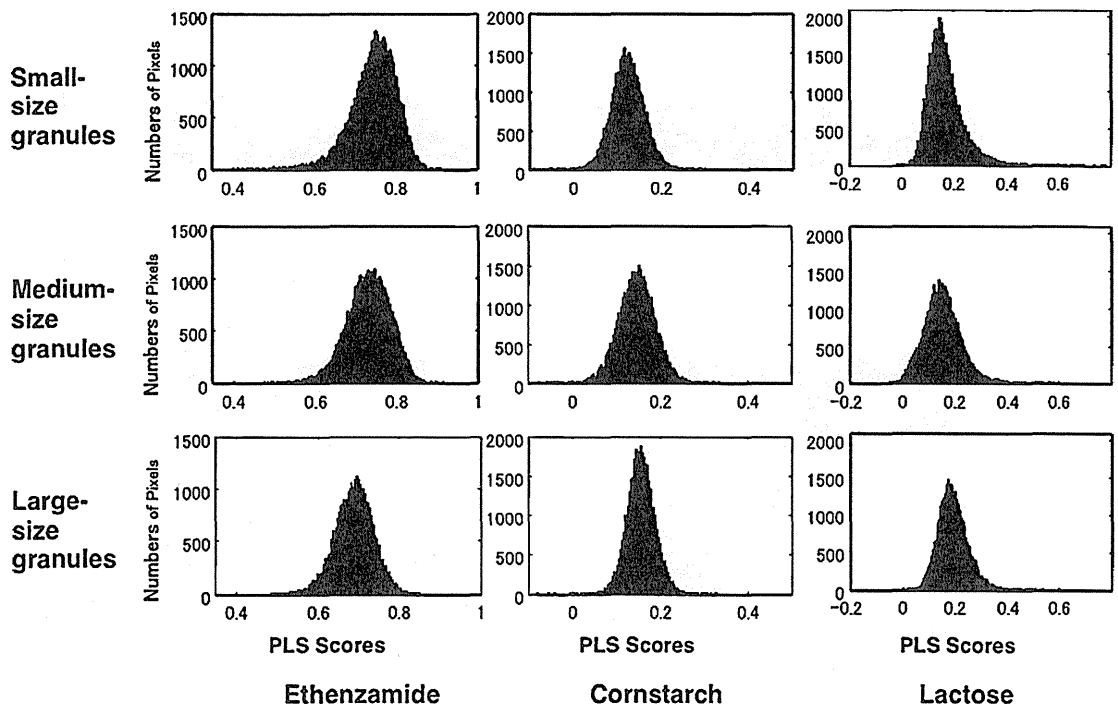

Fig. 8. Associated histograms of the tablets in Fig. 5 (40 rpm, 5 min granulation).

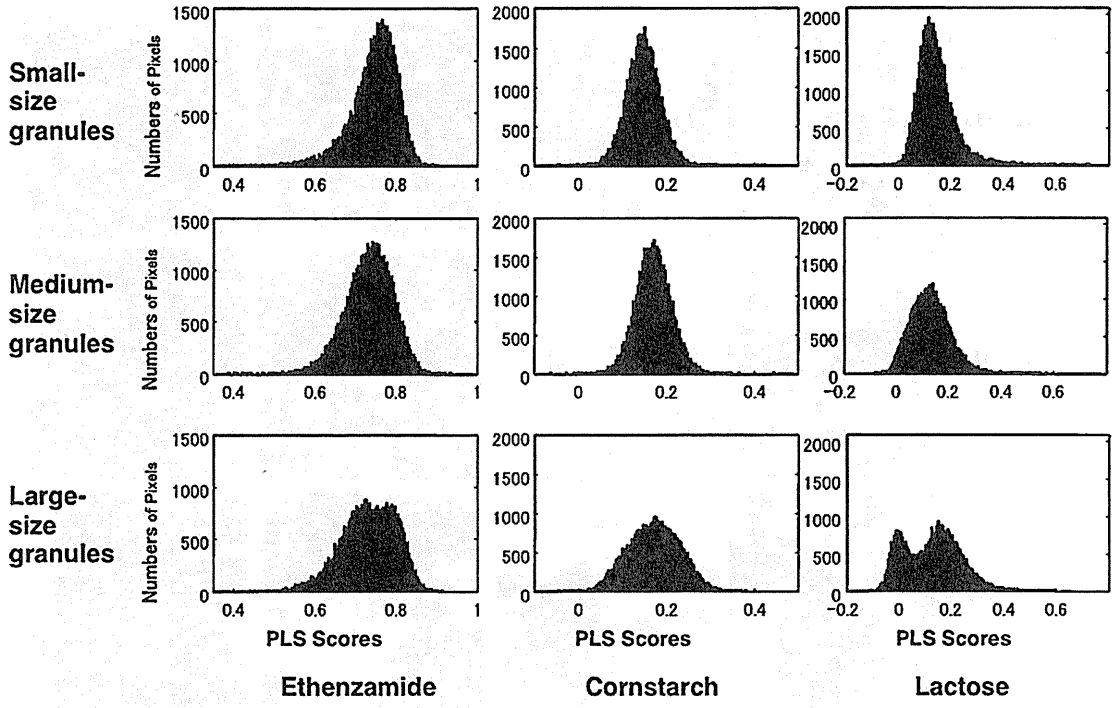

Fig. 9. Associated histograms of the tablets in Fig. 6 (200 rpm, 5 min granulation).

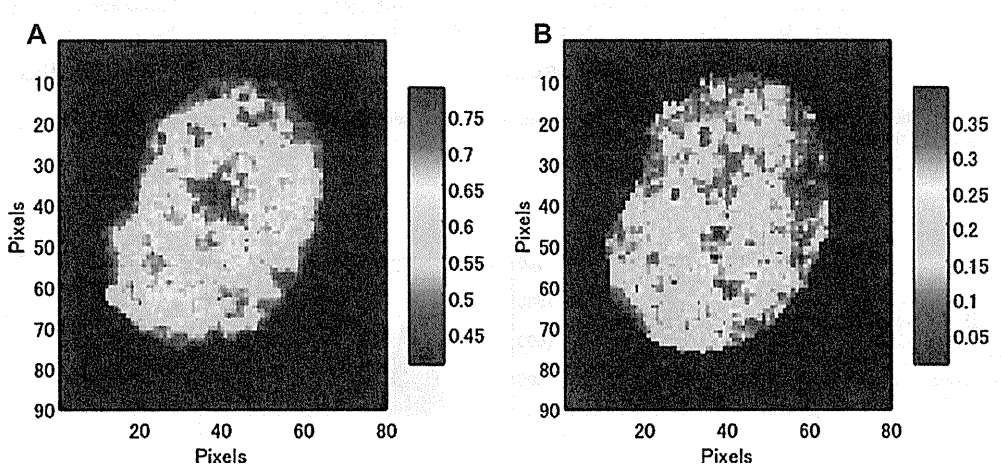

Fig. 10. NIR images of ethenzamide (A) and lactose (B) in granules produced by 5 min of granulation at 40 rpm. For each of the 2 components, the PLS score bar is shown.

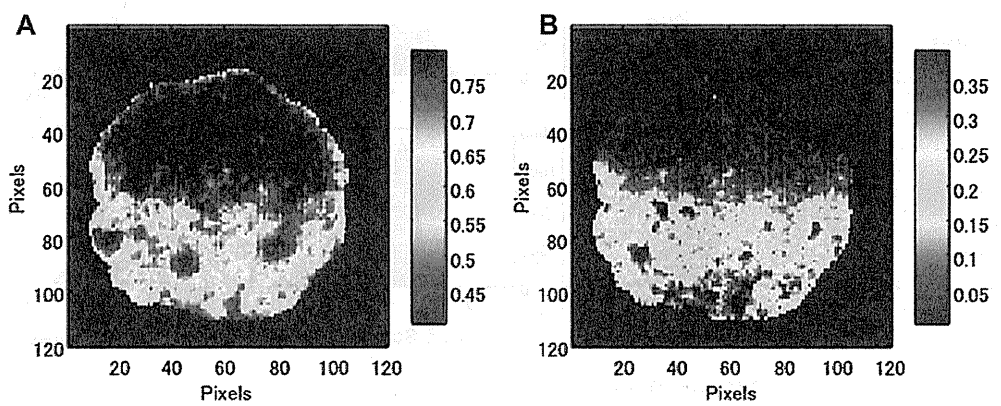

Fig. 11. NIR images of ethenzamide (A) and lactose (B) in granules produced by 5 min granulation at 200 rpm. For each of the 2 components, the PLS score bar is shown.

granulation, eventually reaching an over-granulated state with excessively large granules. We were thus able to produce granules of various qualities for analysis by NIR chemical imaging. We found significant differences in the segregation of ingredients in the experimental tablets when we employed over-granulation conditions using greater impeller rotation speeds and longer granulation times (Figs. 3 and 4). In particular, the lactose domain showed marked agglomeration, which caused the segregation of ingredients. A previous report (Horisawa et al., 2009) indicated that the surface polarity of components was one of the factors influencing the granulation mechanism. We also considered that surface polarity, affecting the affinity between ingredients and water, was one of the important factors in determining the outcome of the granulation process. The formulation we used has a high content of hydrophobic drug (70% ethenzamide) and a low content of hydrophilic lactose. Water added in the granulation process concentrates around the hydrophilic lactose, promoting agglomeration of lactose during granulation. Consequently, hydrophobic ethenzamide and cornstarch were segregated from the agglomerated lactose; the cornstarch and ethenzamide thus tended to migrate together and showed an overlapping distribution in the NIR images. In contrast, no useful information about methylcellulose was obtained by NIR chemical imaging despite its size, which is equivalent to that of ethenzamide and lactose. This may be because methylcellulose became a viscous liquid during granulation, and the resulting domains were too small to detect by NIR imaging.

Segregation seemed to occur in the large-size granules, as it was observed in proportion to the granulation conditions and granule size as D_{50} (Table 2; Figs. 2–4). However, NIR images of tablets made with size-classified granules indicated a large difference in the degree of segregation in large-size granules produced with an impeller speed of 40 rpm compared to that of 200 rpm (Figs. 6 and 7). The associated histograms showed that the degree of homogeneity supported these results (Figs. 8 and 9). In addition, the degree of consolidation of large-size granules differed between those made at impeller speeds of 40 and 200 rpm. This result suggests that the segregation of components occurs during the consolidation step in the granulation process. Over-granulation conditions, such as an impeller speed of 200 rpm and granulation time of 5 min, produced many large and consolidated granules. We

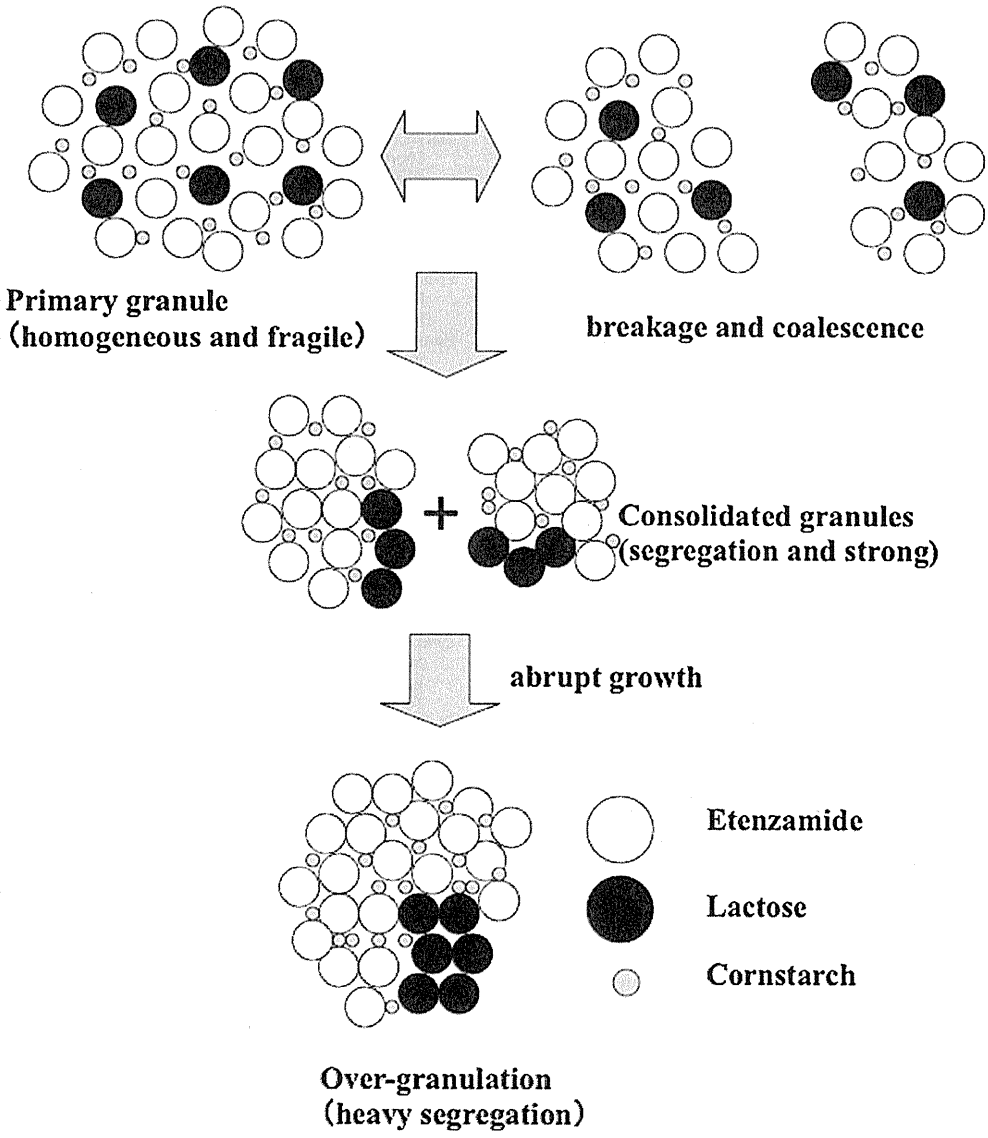

Fig. 12. Proposed model of the segregation process.

were thus able to clearly visualize segregation in the NIR images of tablets made from these granules. In contrast, we observed no segregation in granules and tablets made under appropriate granulation conditions, such as an impeller speed of 40 rpm. These granules were mostly small or medium in size and showed a low rate of consolidation.

Surprisingly, the ethenzamide content in the granules of all sizes were similar to the theoretical values (Table 3), even though segregation of components occurred in the large-size granules. In general, granulation is often employed to improve the homogeneity of solid mixtures. Although it is well-known that the high shear granulation method sometimes produces content inhomogeneity in drug substances made with differently sized granules (Vromans and Van den Dries, 2002), this observation has been attributed to differences in various physical properties, such as the solubility, formulation, or particle size of substances (Oijle et al., 1982; Vromans et al., 1999; Wan et al., 1992). In the present work, however, segregation was observed within the granules (Figs. 10 and 11) and without content inhomogeneity (Table 3). To our knowledge, this phenomenon has not been previously reported. Therefore, our results present novel and significant information about the process of high shear granulation.

From the results of this investigation and knowledge from previous reports on the granulation process, we propose a model for the mechanism of segregation as depicted in Fig. 12. The initial granules that form immediately after adding water are homogeneous. As the initial granules (which are fragile) are repeatedly broken, coalesced, and consolidated by the impeller force, the lactose particles in the granules are agglomerated through the water. Consequently, hydrophobic ethenzamide and cornstarch are segregated from the agglomerated lactose.

In this high load drug formulation model, we detected segregation of components as a result of granulation. However, it should be noted that while this phenomenon occurred with this particular formulation, it might or might not occur in other formulations. Studies of other formulations could contribute information to further advance our understanding of the process of solid dosage form production. Such information could be useful for producing high load drugs, which have tended to present problems in manufacturing.

Real time monitoring is one of the techniques to support quality control in pharmaceutical manufacturing. Shiraishi et al. reported that monitoring of power consumption was useful systems to control the high shear granulation process (Shiraishi et al., 1994, 1995, 1997). These reports showed the granules obtained at point of the first peak in the power consumption curve had the largest pore volumes and were most suitable for manufacturing. Our study showed that the segregation of components found in the consolidated granules that had smaller pore volumes and were unsuitable quality. These results indicate that segregation could be used as an indicator of product quality. However, the segregation observed in this study would not be detectable with conventional analytical technologies such as HPLC, because the content of the granules remained uniform despite the segregation. While monitoring system can detect end point, it does not provide enough detail for use in distribution analysis. In contrast, NIR imaging can be used to determine the distribution of components and to detect segregation in tablets. This information can give answers to quality questions to us. NIR chemical imaging is thus a useful tool for studying granulation.

5. Conclusion

We made the interesting observation that ingredient segregation occurred when over-granulation conditions involving high impeller rotation speeds and long granulation times were used. Ingredients clearly segregated into large and consolidated granules. However, the API content was not affected by the segregation that occurred within the granule. To the best of our knowledge, segregation in granules without content inhomogeneity has not been previously reported. This study therefore presents novel and significant information regarding the process of high shear granulation. Granule visualization using NIR chemical imaging is an effective method for investigating and evaluating the granulation process.

Acknowledgements

The authors thank the US FDA and Pfizer Inc. for providing useful information about NIR imaging, ST Japan Inc. for their technical support, and Shionogi & Co., Ltd. for providing us with starting materials. This work was supported by a grant from the Japan Health Sciences Foundation.

References

Benali, M., Gerbaud, V., Hemati, M., 2009. Effect of operating conditions and physicochemical properties on the wet granulation kinetics in high shear mixer. Powder Technol. 190, 160–169.
Barnes, R.J., Dhanoa, M.S., Lister, S.J., 1989. Standard normal variate transformation and de-trending of near-infrared diffuse reflectance spectra. Appl. Spectrosc. 43, 772–777.
Clarke, F.C., 2004. Extracting process-related information from pharmaceutical dosage forms using near-infrared microscopy. Vib. Spectrosc. 34, 25–35.
Clarke, F.C., Jamieson, M.J., Clark, D.A., Hammond, S.V., Jee, R.D., Moffat, A.C., 2001. Chemical image fusion, the synergy of FT-NIR and Raman mapping microscopy to enable a more complete visualization of pharmaceutical formulations. Anal. Chem. 73, 2213–2220.
Dubois, J., Wolff, J.C., Warrack, J.K., Schoppelrei, J.W., Lewis, E.N., 2007. NIR chemical imaging for counterfeit pharmaceutical product analysis. Spectroscopy 22, 40–50.
El-hagrasy, A.S., Morris, H.R., D'Amico, F., Lodder, R.A., Drennen III, J.K., 2001. Near-infrared spectroscopy and imaging for the monitoring of powder blend homogeneity. J. Pharm. Sci. 90, 1298–1307.
Hammond, S.V., Clarke, F.C., 2002. Near-infrared microspectroscopy. Handbook of Vibrational Spectroscopy, vol. 2. John Wiley and Sons Ltd, pp. 1405–1418.
Horisawa, E., Kobayashi, M., Kawasaki, J., Danjo, K., 2009. Effects of granule characteristics on physical properties of tablet prepared by agitation and fluidized-bet granulation method. J. Pharm. Sci. Technol. Jpn. 69, 228–238.
Iveson, S.M., Litster, J.D., Hapgood, K., Ennis, B.J., 2001. Nucleation, growth and breakage phenomena in agitated wet granulation processes: a review. Powder Technol. 117, 3–39.
Jovanovic, N., Gerich, A., Bouchard, A., Jiskoot, W., 2006. Near-infrared imaging for studying homogeneity of protein–sugar mixtures. Pharm. Res. 23, 2002–2013.
Lewis, E.N., Schoppelrei, J., Lee, E., 2004. Near-infrared chemical imaging and the PAT initiative. Spectroscopy 19, 26–36.
Linda, H., Kidder, L.H., Dubois, J., Lewis, E.N., 2007. Realizing the potential of near-infrared chemical imaging in pharmaceutical manufacturing. Pharmaceut. Sol. Update Spring, 48–52.
Lyon, R.C., Lester, D.S., Lewis, E.N., Lee, E., Yu, L.X., Jefferson, E.H., Hussain, A.S., 2002. Near-infrared spectral imaging for quality assurance of pharmaceutical products: analysis of tablets to assess powder blend homogeneity. AAPS PharmSci Tech 3, 1–15.
Makein, L.J., Kidder, L.H., Lewis, E.N., Valleri, M., 2008. Non-destructive evaluation of manufacturing process changes using near-infrared chemical imaging. NIR News 19, 11–15.
Oijle, J.E., Macfarlane, C.B., Selkirk, A.B., 1982. Drug distribution during massing and its effect on dose uniformity in granules. Int. J. Pharm. 247, 99–107.
Rosipal, R., Krämer, N., 2006. Overview and recent advances in partial least squares. In: Saunders, C., Grobelnik, M., Gunn, S., Shawe-Taylor, J. (Eds.), Subspace, Latent Structure and Feature Selection Techniques. Springer, New York, pp. 34–51.
Saleh, K., Vialatte, L., Guigon, P., 2005. Wet granulation in a batch high shear mixer. Chem. Eng. Sci. 60, 3763–3775.
Shah, R.B., Tawakkul, M.A., Khan, M.A., 2007. Process analytical technology: chemometric analysis of raman and near-infrared spectroscopic data for predicting physical properties of extended release matrix tablets. J. Pharm. Sci. 96, 1356–1365.
Shiraishi, T., Kondo, S., Yuasa, H., Kanaya, Y., 1994. Studies on the granulation process of granules for tableting with a high speed mixer. I. physical properties of granules for tableting. Chem. Pharm. Bull. 42, 932–936.
Shiraishi, T., Sano, A., Kondo, S., Yuasa, H., Kanaya, Y., 1995. Studies on the granulation process of granules for tableting with a high speed mixer. II. Influence of particle size of active substance on granulation. Chem. Pharm. Bull. 43, 654–659.
Shiraishi, T., Kondo, S., Yaguchi, Y., Yuasa, H., 1997. Studies on the granulation process of granules for tableting with a high speed mixer. III. Analysis of the compression process. Chem. Pharm. Bull. 45, 1312–1316.

Sunada, H., Hasegawa, M., Tanino, T., 2003. New expansion of standard formulation research association: inquiry into various problems for dry-molding method by the questionnaires. Pharm. Tech. Jpn. 19, 265–272.
Tanino, T., Tani, M., Nagato, T., Nakamoto, K., Fujimaki, F., Fujiwara, N., Yamane, K., Hashimoto, Y., Hiyama, Y., 2006. PAT application in developing stage. Pharm. Tech. Jpn. 22, 1661–1665.
Vemavarapu, C., Surapaneni, M., Hussain, M., Badawy, S., 2009. Role of drug substance material properties in the processibility and performance of a wet granulated product. Int. J. Pharm. 374, 96–105.
Veronin, M., Youran, B., 2004. Magic bullet gone astray: medications and the Internet. Science 305, 481.
Vonk, P., Guillaume, C.P.F., Ramaker, J.S., Vromans, H., Kossen, N.W.F., 1997. Growth mechanisms of high shear pelletisation. Int. J. Pharm. 157, 93–102.
Vromans, H., Poels-Janssen, H.G.M., Egermann, H., 1999. Effects of high shear granulation on granulate homogeneity. Pharm. Dev. Technol. 4, 297–303.
Vromans, H., Van den Dries, K., 2002. Relationship between inhomogeneity phenomena and granule growth mechanisms in a high shear mixer. Int. J. Pharm. 247, 167–177.
Wan, L.S.C., Heng, P.W.S., Muhurie, G., 1992. Incorporation and distribution of a low dose drug in granules. Int. J. Pharm. 88, 159–163.
Westenberger, B.J., Ellison, C.D., Fussner, A.S., Jenney, S., Kolinski, T.G., Lipe, T.G., Lyon, R.C., Moore, T.W., Revelle, L.K., Smith, A.P., Spencer, J.A., Story, K.D., Toler, D.Y., Wokovich, A.M., Buhse, L.F., 2005. Quality assessment of Internet pharmaceutical products using traditional and non-traditional analytical techniques. Int. J. Pharm 306, 56–70.

European Journal of Pharmaceutics and Biopharmaceutics 85 (2013) 177–183

Contents lists available at SciVerse ScienceDirect

European Journal of Pharmaceutics and Biopharmaceutics

journal homepage: www.elsevier.com/locate/ejpb

Research paper

Impact of heat treatment on miscibility of proteins and disaccharides in frozen solutions

Ken-ichi Izutsu [a,*], Chikako Yomota [a], Haruhiro Okuda [a], Toru Kawanishi [a], Theodore W. Randolph [b], John F. Carpenter [c]

[a] National Institute of Health Sciences, Tokyo, Japan
[b] Department of Chemical and Biological Engineering, University of Colorado, Boulder, CO, USA
[c] Department of Pharmaceutical Sciences, University of Colorado Denver, Aurora, CO, USA

ARTICLE INFO

Article history:
Available online 18 May 2013

Keywords:
Protein formulation
Stability
Phase separation
Freeze-concentration
Heat treatment
Freeze-drying

ABSTRACT

The purpose of this study was to elucidate the effect of heat treatment (annealing) on the miscibility of concentrated protein and disaccharide mixtures in the freezing segment of lyophilization. Frozen solutions containing a protein (e.g., recombinant human albumin, chicken egg lysozyme, bovine plasma immunoglobulin G, or a humanized IgG1k monoclonal antibody) and a non-reducing disaccharide (e.g., sucrose or trehalose) showed single thermal transitions of the solute mixtures (glass transition temperature of maximally freeze-concentrated solutes: T'_g) in their first heating scans. Heat treatment (e.g., −5 °C, 30 min) of some disaccharide-rich mixture frozen solutions at temperatures far above their T'_g induced two-step T'_g transitions in the subsequent scans, suggesting the separation of the solutes into concentrated protein–disaccharide mixture phase and disaccharide phase. Other frozen solutions showed a single transition of the concentrated solute mixture both before and after heat treatment. The apparent effects of the heat treatment temperature and time on the changes in thermal properties suggest molecular reordering of the concentrated solutes from a kinetically fixed mixture state to a more thermodynamically favorable state as a result of increased mobility. The implications of these phenomena on the quality of protein formulations are discussed.

1. Introduction

The commercial development of recombinant protein pharmaceuticals requires rational formulation design to retain protein stability throughout the production process and clinical use [1,2]. Freeze-drying is an effective method of achieving an acceptable shelf life (e.g., 24 months) for chemically and/or physically unstable proteins. While the removal of water by lyophilization reduces the rate of protein chemical degradation during storage, the process often induces irreversible protein aggregation due to higher-order structural changes. The structurally-altered protein molecules are also more susceptible to various types of chemical degradation during storage [3]. To prevent the lyophilization-induced protein unfolding, many protein formulations contain non-reducing disaccharides (e.g., sucrose and trehalose) that substitute surrounding water molecules and provide a glassy matrix, which is required for long-term protein storage stability in dried solids [1,4]. Low-molecular-weight saccharides reduce protein denaturation in aqueous solutions and during freezing because they are preferentially excluded from the surface of the proteins; they also increase the free energy of protein unfolding by elevating the chemical potential of the unfolded state above that of the native state [5–7]. The increasing clinical relevance of lyophilized protein pharmaceuticals highlights the importance of understanding various factors that determine the formulation quality and the efficiency of the typical long high-energy process.

In the first step of lyophilization, freezing to form crystals of pure water concentrates the remaining solutes into a highly viscous solution [8,9]. Some solutes tend to crystallize in frozen solutions, while others are kinetically trapped in the concentrated supercooled liquids. Multiple solutes in lyophilized pharmaceutical formulations can be miscible or immiscible in the freeze-concentrates, depending on the particular combination, concentration ratio, and freezing process [10–16]. The multiple concentrated solute phases should form during the freezing process and upon exposure of the frozen solutions to higher temperatures. Freeze-concentration separates some polymer combinations, such as dextran and polyvinylpyrrolidone (PVP) or ovalbumin and PVP (in the presence of NaCl), from miscible lower-concentration aqueous solutions into multiple non-crystalline phases rich in one of the polymers by the same thermodynamic mechanism that induces aqueous two-layer

* Corresponding author. National Institute of Health Sciences, Kamiyoga 1-18-1, Setagaya 158-8501, Tokyo, Japan. Tel.: +81 337001141; fax: +81 337076950.
E-mail address: izutsu@nihs.go.jp (K.-i. Izutsu).

0939-6411/$ - see front matter © 2013 Elsevier B.V. All rights reserved.
http://dx.doi.org/10.1016/j.ejpb.2013.05.004

systems [10,14,16,17]. This phase separation influences the physical properties of the frozen solutions and the resulting material post-drying (e.g., multiple transitions and varied propensity for physical collapse) [18,19]. Many other formulation ingredients tend to be freeze-concentrated without these apparent phase separations [20].

The miscibility of proteins and non-reducing disaccharides in frozen solutions and freeze-dried solids is of particular interest in formulation development. Several preceding studies utilizing thermal analysis and spectroscopic methods (e.g., Raman and near-infrared mapping, FT-IR) suggest non-ideal mixing of proteins and disaccharides in freeze-dried solids; however, available information is still limited partly because of the microporous and hygroscopic nature of these cakes [13,20–27]. Raman microscopy analysis of frozen solutions also revealed variable distributions of lysozyme and trehalose in freeze-concentrated liquid and ice regions [28]. Our previous study indicated contribution of thermal history on the miscibility of some solutes in frozen solutions [25]. For example, a nonionic polymer (e.g., dextran) and a disaccharide (e.g., trehalose) that are initially concentrated into a mixture supercooled phase upon ice formation, separate into saccharide-rich and solute mixture freeze-concentrated phases upon heat treatment of frozen solutions at temperatures far above the glass transition temperature of maximally freeze-concentrated solutes (T'_g). The composition of solutes in the resulting non-crystalline phases depends largely on the consisting polymers. The post-freezing heat treatment (i.e., annealing) is gaining increasing attention as a method for reducing the ice-subliming primary drying segment time and also the inter-batch and inter-vial heterogeneity in drying behavior. The ice crystal size growth by coalescence (Ostwald ripening) and the resulting larger connecting pores in the dried solid layers often facilitate faster ice sublimation. The method would be particularly valuable for drying biopharmaceutical formulations since many disaccharide-containing frozen solutions have a relatively low "maximum allowable product temperature" to avoid the physical collapse of the products [29].

There is a reasonable chance that the increasing solute mobility during exposure of frozen solutions to temperatures far above the T'_g alters the miscibility of the concentrated proteins and disaccharides. Therefore, in the present study, we performed thermal analysis to investigate the effects of heat treatment on the miscibility of proteins and disaccharides in frozen solutions. Recombinant human albumin, egg yolk lysozyme, bovine immunoglobulin G, and a humanized monoclonal antibody were used as model proteins. Temperature profiles of the thermal transition (T'_g) provided valuable information on solute miscibility in freeze-concentrates.

2. Materials and methods

2.1. Materials

All chemicals employed in this study were of analytical grade and were obtained from the following commercial sources: sucrose, D-(+)-trehalose dihydrate, and recombinant human albumin (rHA, A9731; Sigma–Aldrich, St. Louis, MO); bovine plasma immunoglobulin G (bIgG, 641401; MP Biomedicals, Solon, OH); L-histidine, L-histidine hydrochloride monohydrate, disodium hydrogenphosphate, and sodium dihydrogenphosphate dihydrate (Wako Pure Chemical Industries, Osaka, Japan); and egg yolk lysozyme (Seikagaku, Tokyo, Japan). A commercial recombinant DNA-derived humanized IgG1k monoclonal antibody (mAbA) lyophilized formulation was also used in the study. The bIgG and mAbA were dialyzed overnight against a histidine-HCl buffer (5 mM, pH 7.0) containing 100 mM NaCl. Other proteins were dialyzed against the buffer without NaCl. The concentrations of the proteins were determined from the absorbance at 280 nm by using the appropriate extinction coefficient for each protein.

2.2. Thermal analysis of frozen solutions and freeze-dried solids

Thermal analysis of the frozen solutions was performed using a differential scanning calorimeter (DSC Q-10; TA Instruments, New Castle, DE) and Universal Analysis software (TA Instruments). All solutions used in the thermal analysis were single-phase at room temperature. Aliquots of aqueous solutions (10 μL) in aluminum cells were cooled from room temperature to −70 °C at 10 °C/min. The first heating scan of the frozen solutions at 5 °C/min was paused at various temperatures (−25 to −5 °C, −5 °C unless otherwise mentioned) and then maintained at the temperature for various times (1–480 min, 30 min unless otherwise mentioned). After annealing, the solutions were cooled to −70 °C and then heated at a rate of 5 °C/min. The first derivative of the thermograms was calculated to increase the sensitivity of detection of the thermal events (e.g., T'_g). The T'_g was estimated as the temperature at which the highest peak in the derivative thermogram appeared. The two-step heat flow changes observed in the first and second scans of some heat-treated frozen solutions were provisionally described as lower- (T'_{g1L}, T'_{g2L}) and higher temperature (T'_{g1H}, T'_{g2H}) transitions.

3. Results

3.1. Effects of heat treatment on albumin and disaccharide miscibility

Fig. 1 shows the derivative thermograms of frozen solutions containing rHA and trehalose at various concentration ratios (total 200 mg/mL) obtained in the heating scans prior to and after heat treatment at −5 °C for 30 min. An exotherm attributed to ice crystallization was observed during cooling between −15 and −25 °C (data not shown). The frozen trehalose solution showed a peak that

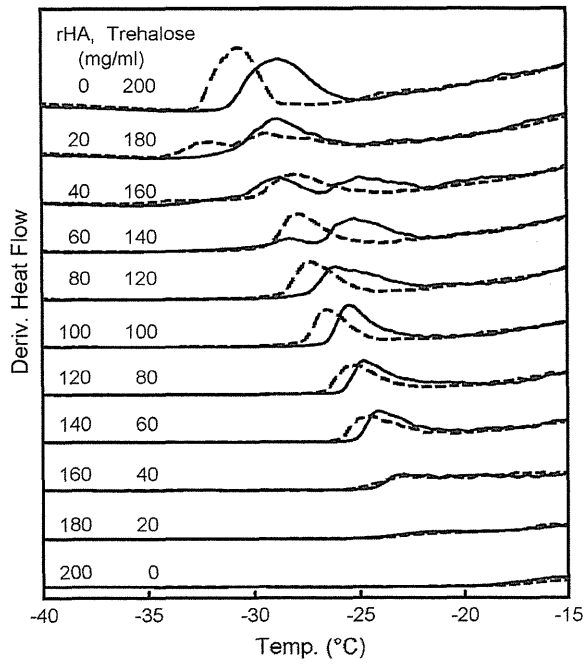

Fig. 1. Derivative thermograms of frozen solutions containing various concentration ratios of rHA and trehalose (total 200 mg/mL, 5 mM histidine-HCl buffer, pH 7.0, 10 μL) obtained in the heating scans (5 °C/min) prior to (first scans, dotted lines) and after (second scans, solid lines) heat treatment at −5 °C for 30 min.